Dark Mass is Potential Energy

Nicolas Poupart
Independent Researcher (2025)
99 Chemin Scraire, Mille-Isles, Québec, Canada (J0R 1A0)
(450) 939-2167
nicolas.poupart@yahoo.fr

Abstract

This paper demonstrates that gravitational potential energy ($E = -GmM/d$) accounts for the phenomenon commonly attributed to dark matter, by applying the mass–energy equivalence relation ($E = mc^2$). No additional assumptions are made beyond the principle of volume conservation, ensuring that the gravitational field remains conservative and uninfluenced by forces other than gravity. We develop a straightforward equation and algorithm to accurately compute the potential energy of a stellar system. The theoretical implications of this model are explored with respect to energy production by various types of stars and black holes in galaxies. The model is empirically tested against the SPARC database comprising 175 galaxies to assess its validity. We continue by verifying that our model reproduces the total galactic and extragalactic dark mass and is compatible with ΛCDM cosmology. Then we demonstrate that the experimental adequacy of our model reaches 5σ. We derive the logical consequences of the potential energy stored in the gravitational field; a claim validated by SPARC data. We conclude that, to ensure the consistency of our model across the entire cosmic history, it is necessary to impose the conservation of the cosmological energy balance.

Introduction

Since Vera Rubin postulated the existence of galactic dark mass to explain the flatness of galactic rotation curves [1, 2, 3], no convincing explanation for the nature of this mass has been provided. Attempts to attribute the missing mass to undetectable baryonic matter were largely refuted by the AGAPE [4], MACHO [5], and EROS [6] programs. Similar explanations involving non-baryonic or exotic particles have also failed to account for the discrepancy. Numerous detection efforts, including those by the LUX [7], PICASSO [8], PICO [9], and SuperCDMS [10] collaborations, have thus far been unsuccessful. Likewise, results from CERN's latest accelerator suggest that physics remains consistent with the Standard Model, making the existence of exotic particles increasingly unlikely. It also remains extremely difficult to explain this phenomenon using current gravitational theory, whether Newtonian gravitation or general relativity.

In cosmology, the prevailing framework is the ΛCDM model, which postulates the existence of cold dark matter. For most physicists, the concept of mass remains inseparable from that of matter. Moreover, the term "dark matter" is often used categorically, although it more accurately refers to "dark mass". One alternative to the existence of real dark mass is to modify gravitation at galactic scales. However, such efforts are challenged by the remarkable empirical adequacy of general relativity in describing observed phenomena and the inferred presence of dark mass [11, 12, 13].

The explanation proposed in this article takes a fundamentally different approach. Dark mass is neither a form of real matter nor the result of modified gravitation. Rather, it is a secondary effect inherent to the current formulation of gravitational theory—specifically, the gravitational potential energy stored in the field. The only axioms employed are $E = -GmM/d$ and $E = mc^2$. Thus, the explanation relies solely on the judicious application of classical physics.

Useful Gravitational Potential Energy

If we consider the Newtonian gravitational force equation, $F = GmM/d^2$, we obtain—by integrating from d to infinity—the potential energy formula $E_p = -GmM/d$. While this formulation yields negative potential energy which can be used for calculating the motion of celestial bodies, it is unsuitable for evaluating the total physical potential energy of a system.

To determine the physically meaningful potential energy, we must compute the energy difference between two states of the system—analogous to lifting a mass m from position d by a height h. In such a case:

$$\Delta E_p = E_p(d+h) - E_p(d) = \frac{GmMh}{d^2 + dh}$$

This expression represents the usable form of gravitational potential energy. The concept of absolute negative energy E_p is not directly interpretable in physical terms.

However, this formulation becomes impractical for systems involving two celestial bodies (e.g., planets, stars, or galaxies), because the initial reference distance d is undefined or ambiguous. To resolve this, we compute the energy difference between a compact state—a single solid spherical mass $M_t = m+M$—and a configuration of two distinct spherical bodies, m and M, separated by a distance d.

Let the two bodies have radii r and R, and volumes $v = 4\pi r^3/3$ and $V = 4\pi R^3/3$, with corresponding densities m/v and M/V. The total volume of the single solid sphere is $V_t = V+v = 4\pi(R^3+r^3)/3$, and its radius $R_t = (R^3+r^3)^{1/3}$. Assuming equal volumetric densities, $m/v = M/V$, that of the single compact ball will be identical: $m/v = M/V = M_t/V_t$; if not, it assumes an average density weighted by the contributions of m and M.

The gravitational potential energy of a homogeneous solid sphere is given by:

$$E_p = -\frac{3GM^2}{5R}$$

The gravitational potential energy of the system can be evaluated by comparing the initial state (a single compact mass), the final state (two separated masses), and the difference between them:

$$E_i = -\frac{3GM_t^2}{5R_t}$$
$$E_f = -\frac{3GM^2}{5R} - \frac{3Gm^2}{5r} - \frac{GMm}{d}$$
$$\Delta E_p = E_f - E_i = \left(-\frac{3GM^2}{5R} - \frac{3Gm^2}{5r} - \frac{GMm}{d}\right) + \frac{3GM_t^2}{5R_t}$$

This expression quantifies the energy change from a compact configuration to a system of two separated masses. It represents a redistribution of matter that preserves the original component densities, thereby ensuring that the transformation involves only gravitational forces.

Gravitational Potential Energy is Massive

Gravitational potential energy can be expressed as $E_p = m_p c^2$, indicating that it must be stored as mass within the system. This statement is readily illustrated through a simple thought experiment. Consider a nuclear reactor that converts a mass m_n into electrical energy, which is then used to raise a mass m to a height h.

There should be no debate regarding whether the Earth's mass remains unchanged before and after the transformation. Given the conservation of mass–energy m_n within the Earth system, general relativity ensures that its gravitational field remains unchanged. The question of whether this constitutes "real" mass is meaningless, since mass is defined by its measurable gravitational or inertial effects. However, this new mass does not in turn generate potential energy *ad infinitum*; if such a principle of self-induction were to exist in the field, the Newtonian calculation would merely be the limiting sum.

Moreover, since the equivalence of inertial and gravitational mass has never been empirically violated [14], we may, for now, treat gravitational potential energy as fully equivalent to its mass representation.

Calculation of the Potential Energy of Celestial Bodies

Table 1: Physical parameters for celestial body pairs

System	m (kg)	M (kg)	r (m)	R (m)	d (m)	R_t (m)
Moon+Earth	$7.35 \cdot 10^{22}$	$5.97 \cdot 10^{24}$	$1.74 \cdot 10^{6}$	$6.38 \cdot 10^{6}$	$3.8 \cdot 10^{8}$	$6.42 \cdot 10^{6}$
Earth+Sun	$5.97 \cdot 10^{24}$	$1.99 \cdot 10^{30}$	$6.38 \cdot 10^{6}$	$6.96 \cdot 10^{8}$	$1.5 \cdot 10^{11}$	$6.96 \cdot 10^{8}$
Jupiter+Sun	$1.90 \cdot 10^{27}$	$1.99 \cdot 10^{30}$	$6.99 \cdot 10^{7}$	$6.96 \cdot 10^{8}$	$7.8 \cdot 10^{11}$	$6.97 \cdot 10^{8}$
Sun+M80	$1.99 \cdot 10^{30}$	$9.99 \cdot 10^{35}$	$6.96 \cdot 10^{8}$	$5.53 \cdot 10^{10}$	$4.5 \cdot 10^{17}$	$5.53 \cdot 10^{10}$
Sun+Galaxy	$1.99 \cdot 10^{30}$	$5.00 \cdot 10^{40}$	$6.96 \cdot 10^{8}$	$2.04 \cdot 10^{12}$	$5.0 \cdot 10^{20}$	$2.04 \cdot 10^{12}$

Table 1 contains the standard values for the celestial bodies under consideration, except for the radii for the globular cluster M80 and a representative galaxy. We modeled the initial state as a solid sphere of mass $M + m$, assuming solar density. The final state is the Sun at distance d of a mass M of solar density. For the Sun-M80 pair, the values used are $R = 5.534217 \cdot 10^{10}$, $R_t = 5.534221 \cdot 10^{10}$ and for the Sun-galaxy pair, the values used are $R = 2.03985712710655 \cdot 10^{12}$ and $R_t = 2.03985712713359 \cdot 10^{12}$. The rationale behind this construction will be addressed in a subsequent section. In either case, the radius is calculated using the relation $R_t = (R^3 + r^3)^{1/3}$.

Table 2: Gravitational potential energy differences and mass equivalents

System	E_i (J)	E_f (J)	ΔE_p (J)	ΔE_p (kg)	$m/\Delta E_p$
Moon+Earth	$-2.2795 \cdot 10^{32}$	$-2.2413 \cdot 10^{32}$	$3.8176 \cdot 10^{30}$	$4.2477 \cdot 10^{13}$	$1.0 \cdot 10^{-9}$
Earth+Sun	$-2.2751 \cdot 10^{41}$	$-2.2751 \cdot 10^{41}$	$1.3024 \cdot 10^{36}$	$1.4491 \cdot 10^{19}$	$2.4 \cdot 10^{-6}$
Jupiter+Sun	$-2.2787 \cdot 10^{41}$	$-2.2751 \cdot 10^{41}$	$3.5519 \cdot 10^{38}$	$3.9520 \cdot 10^{21}$	$2.1 \cdot 10^{-6}$
Sun+M80	$-7.2141 \cdot 10^{50}$	$-7.2141 \cdot 10^{50}$	$2.3949 \cdot 10^{45}$	$2.6647 \cdot 10^{28}$	$1.34 \cdot 10^{-2}$
Sun+Galaxy	$-4.9079 \cdot 10^{58}$	$-4.9079 \cdot 10^{58}$	$3.2540 \cdot 10^{48}$	$3.6206 \cdot 10^{31}$	18.2

Table 2 presents the gravitational potential energy differences between current physical configurations and their hypothetical fusion into a single mass. For context, the complete annihilation of one kilogram of matter yields an energy output approximately equivalent to that of a hydrogen bomb. For example, 2 kg of deuterium fused with 3 kg of tritium results in a mass loss of roughly 1 kg—comparable to the energy released by the Tsar Bomba.

Based on this equivalence, the merger of the Moon with the Earth would release energy equivalent to approximately 40 trillion hydrogen bombs. This potential energy corresponds to a mass of about 40 billion metric tons—a value that is far from negligible.

If we consider the energy released by merging the Earth into the Sun, the resulting energy would correspond to over 14 million billion metric tons. However, this value is still less than the mass the Sun loses each hour due to nuclear fusion. Depending on its spatial distribution, this energy-equivalent mass could, in principle, be measurable.

If we examine the ratio $m/\Delta E_p$, representing the mass of the smaller body relative to the potential energy of the system, we find that it is negligible in most cases—except at the galactic scale, where it approaches the order of magnitude of the observed dark mass ratio.

The Potential Energy of Celestial Systems

The first observation is that the term $-GmM/d$ of ΔE_p is negligible at all relevant scales, where $d \gg R \gg r$. This result is intuitive from a physical standpoint, altering the distance between two celestial bodies, such as the Earth and the Moon, leads to minimal changes in gravitational energy compared to the energy released by their hypothetical fusion. This approximation holds across all celestial systems.

The energy expression thus simplifies to:

$$\Delta E_p = \frac{3G}{5}\left(\frac{M_t^2}{R_t} - \frac{M^2}{R} - \frac{m^2}{r}\right)$$

This implies that the spatial arrangement of bodies relative to one another is irrelevant for calculating total gravitational potential energy. If we consider a system of n masses m_i with radii r_i, merged sequentially, we obtain the following expressions:

$$M_i = \sum_{j\leq i} m_j, \quad R_i = \left(R_{i-1}^3 + r_i^3\right)^{1/3}$$

$$\Delta E_i = \frac{3G}{5}\left(\frac{M_i^2}{R_i} - \frac{M_{i-1}^2}{R_{i-1}} - \frac{m_i^2}{r_i}\right), \quad \Delta E_p = \sum_{i\leq n} \Delta E_i$$

It is important to note that the order of mergers is irrelevant, as the gravitational field is conservative. This is verified mathematically.

Proof of Permutation Invariance — Let σ be any permutation of $\{1, \ldots, n\}$. Setting:

$$M_i \equiv M_{i-1} + m_{\sigma(i)}, \qquad R_i^3 \equiv R_{i-1}^3 + r_{\sigma(i)}^3, \qquad M_0 = R_0 = 0$$

we define:

$$\Delta E_i \;=\; \frac{3G}{5}\left(\frac{M_i^2}{R_i} - \frac{M_{i-1}^2}{R_{i-1}} - \frac{m_{\sigma(i)}^2}{r_{\sigma(i)}}\right)$$

The telescopic sum gives:

$$\sum_{i=1}^{n} \Delta E_i \;=\; \frac{3G}{5}\left(\frac{M_n^2}{R_n} - \sum_{i=1}^{n} \frac{m_{\sigma(i)}^2}{r_{\sigma(i)}}\right) \;=\; \frac{3G}{5}\left(\frac{M_{\text{tot}}^2}{R_{\text{tot}}} - \sum_{i=1}^{n} \frac{m_i^2}{r_i}\right)$$

because $M_n = \sum_{i=1}^n m_{\sigma(i)} = \sum_{i=1}^n m_i \equiv M_{\text{tot}}$ and:

$$R_n^3 = \sum_{i=1}^{n} r_{\sigma(i)}^3 = \sum_{i=1}^{n} r_i^3 \;\Rightarrow\; R_{\text{tot}} = \left(\sum_{i=1}^{n} r_i^3\right)^{1/3}$$

The final expression does not depend on σ; thus $\Delta E_p = \sum_{i=1}^n \Delta E_i$ is invariant to the order of mergers.

Simplified Calculation with Identical Mass and Radius

By assuming identical mass m and radius r for each of the n bodies, the calculation simplifies considerably. In this case, the cumulative mass at the ith merger step is $M_i = im$, and the corresponding radius is:

$$\frac{M_i}{V_i} = \frac{m}{v} \Rightarrow R_i = \left(\frac{M_i r^3}{m}\right)^{1/3}$$

since M_i retains the same density as the original body of mass m.

The change in gravitational potential energy at each step is given by:

$$\Delta E_i = \frac{3G}{5}\left(\frac{M_i^2}{R_i} - \frac{M_{i-1}^2}{R_{i-1}} - \frac{m^2}{r}\right), \quad \Delta E_p = \sum_{i \le n} \Delta E_i$$

Due to cancellation of intermediate terms, the telescoping sum simplifies to:

$$\Delta E_p = \frac{3G}{5}\left(\frac{M_n^2}{R_n} - n\frac{m^2}{r}\right)$$

Since $M_n = nm$, we find:

$$M_n^2 = n^2 m^2 \quad \text{and} \quad R_n = \left(\frac{M_n r^3}{m}\right)^{1/3} = n^{1/3} r$$

Substituting into the equation:

$$\Delta E_p = \frac{3G}{5}\left(\frac{n^2 m^2}{n^{1/3} r} - \frac{n m^2}{r}\right) = \frac{3G}{5}\left(n^{5/3} - n\right)\frac{m^2}{r}$$

This final expression shows that the total gravitational potential energy of the system depends solely on the mass, radius, and number of individual bodies. Consequently, a small radius and large mass—i.e., high density—of the component solid spheres significantly increases the total potential energy of the system.

Practical Estimation from a Stellar Population Histogram

In practice, the stellar population of a galaxy is typically known through a mass distribution histogram. The total stellar mass M can be partitioned into k discrete intervals, each denoted by a triplet (M_i, m_i, r_i), where $M_i = n_i m_i$ represents the cumulative mass, m_i the individual stellar mass, and r_i the stellar radius.

The first step involves calculating the contribution from each interval as:

$$\Delta E_{\text{pa}} = \sum_{i \le k} \frac{3G}{5}\left(\frac{M_i^2}{R_i} - n_i \frac{m_i^2}{r_i}\right), \quad R_i = \left(\frac{M_i r_i^3}{m_i}\right)^{1/3}$$

Next, we compute the residual potential energy ΔE_{pb} by merging all k compact balls (M_i, R_i). The total gravitational potential energy of the system is then:

$$\Delta E_p = \Delta E_{\text{pa}} + \Delta E_{\text{pb}}$$

Alternatively, this process can be formalized via a function $f(m, r, M, M_i, R_i) \to (\Delta E_{pi}, M_t, R_t)$ which takes as input the mass m, radius r, and total mass M of the stellar units, along with an optional compact configuration (M_i, R_i) that may be initialized to zero. The function returns the total potential energy for the interval ΔE_{pi}, along with the updated total mass M_t and radius R_t, with $\Delta E_p = \Delta E_p + \Delta E_{pi}$.

Algorithm

$$f(m, r, M, M_i, R_i) \rightarrow \left\{ \begin{array}{ll} n & = \dfrac{M}{m} \\ M_t & = M + M_i \\ R & = n^{1/3} \cdot r \\ R_t & = \left(R^3 + R_i^3\right)^{1/3} \\ \Delta E_{\text{pi}} & = \dfrac{3G}{5}\left(\dfrac{M_t^2}{R_t} - \dfrac{n \cdot m^2}{r}\right) \end{array} \right\} \rightarrow (\Delta E_{\text{pi}}, M_t, R_t)$$

Since the term $n \cdot m^2/r$ is negligible (see the next section "the initial compact configuration") then knowing the density $\rho = m/v$ it is possible to simplify the algorithm:

$$f(\rho, M, M_i, R_i) \rightarrow \left\{ \begin{array}{ll} M_t & = M + M_i \\ R & = \left(\dfrac{3M}{4\pi\rho}\right)^{1/3} \\ R_t & = \left(R^3 + R_i^3\right)^{1/3} \\ \Delta E_{\text{pi}} & = \dfrac{3GM_t^2}{5R_t} \end{array} \right\} \rightarrow (\Delta E_{\text{pi}}, M_t, R_t)$$

The Initial Compact Configuration

We define the initial compact configuration as a solid sphere that conserves the total volume of the bodies it replaces. This strict conservation of volume ensures the physical consistency of the state of matter before and after compaction. Given the difference in potential energy between a final dilute state and an initial compact state, it is possible to simplify this expression:

$$\Delta E_p = \frac{3G}{5}\left(\frac{M_n^2}{R_n} - n\frac{m^2}{r}\right)$$

Since $M_n = nm$, we have:

$$M_n^2 = n^2 m^2 \quad \text{and} \quad R_n = \left(\frac{M_n r^3}{m}\right)^{1/3} = n^{1/3} r$$

Substituting into the equation:

$$\Delta E_p = \frac{3G}{5}\left(\frac{n^2 m^2}{n^{1/3} r} - \frac{n m^2}{r}\right) = \frac{3G}{5}\left(n^{5/3} - n\right)\frac{m^2}{r}$$

The asymptotic behavior shows that for $n \gg 1$, the $n^{5/3}$ term dominates over n, justifying the approximation:

$$\Delta E_p \approx \frac{3G}{5} \cdot \frac{M_n^2}{R_n}$$

Therefore, the potential energy of the dilute structure is strictly equivalent to that of the compact structure. Thus, if the compact ball M_n, or a corresponding dilute system, collapses into a black hole, its potential energy ΔE_p will be entirely emitted in radiation. Indeed, the final black hole of mass M_n has no potential energy in the classical sense and is entirely defined by its mass, spin, and charge. The transition from the compact ball to the black hole therefore requires the loss of its potential energy.

We can therefore distinguish two types of energy regime: those whose critical mass will necessarily push it to collapse into a black hole, and the others. Thus, the ratio $E_{\rm rad}/\Delta E_p$ of the radiation emission of a kilo of sand collapsing into a compact ball will be practically zero, while that of the hypothetical collapse of a galaxy is strictly equal to one.

The compact solid sphere, conserving volumes, is the state of maximum entropy of maximum energy, while the black hole is the state of maximum entropy of minimum energy.

The fact that the compact ball conserving volumes corresponds to the state of maximum total potential energy is simply the consequence of the action-reaction principle and the conservation of energy. This is the most compact state that does not introduce additional repulsive forces, such as degeneracy pressure or radiation pressure, beyond those already present in the low-density state. It is enough to imagine this compact ball as simply being, for example, all the stars of a galaxy placed side by side. In such a configuration, all the forces are conserved. This conservation of forces is strictly necessary to keep the total energy of the system intact.

Hierarchical Calculation of Gravitational Potential Energy

We aim to estimate the gravitational potential energy ΔE_p of large-scale structures by performing a hierarchical construction of sources. In the weak-field regime (relevant for galaxies, groups, and clusters), General Relativity reduces to the cosmological Poisson equation:

$$\nabla^2 \Phi^{(\ell)} \simeq 4\pi G\, a^2\, \delta\rho_b^{(\ell)}$$

where $\delta\rho_b^{(\ell)}$ is the baryonic overdensity smoothed at scale ℓ, and $\Phi^{(\ell)}$ is the corresponding potential. The potential energy at this scale is then given, equivalently, by:

$$\Delta E_p^{(\ell)} = -\frac{1}{2}\int \rho_b^{(\ell)}\, \delta\Phi^{(\ell)}\, \mathrm{d}^3x \quad \text{or} \quad \Delta E_p^{(\ell)} \simeq -\frac{G}{2}\sum_{i\neq j}\frac{m_i^{(\ell)} m_j^{(\ell)}}{r_{ij}}$$

To avoid any double-counting, the effective dark mass inferred at a given scale is never reinjected as a source at the next higher scale. Physically, all forms of mass/energy gravitate in General Relativity; here, this is a bookkeeping convention that allows the inference of a dark component from baryons without recursive feedback.

Changing scale implies a change in the effective density of inhomogeneities:

- **Galactic Scale** ($\ell_{\rm gal} \sim$ kpc). The elementary building blocks are stars, characterized by their masses and internal densities. We compute $\Delta E_p^{\rm gal}$ using $\rho_b^{(\ell_{\rm gal})}$ (the stellar population), and, if necessary, define an effective galactic dark mass $M_{\rm gblk}$.

- **Extragalactic Scale** ($\ell_{\rm exgal} \sim$ Mpc). The building blocks now become galaxies themselves, modeled as compact solid spheres resulting from the lower-level hierarchical calculation. We compute $\Delta E_p^{\rm exgal}$ between galaxies (clusters, filaments) through the fusion of these galactic solid spheres, and from this one may, if desired, infer an effective extragalactic dark mass $M_{\rm eblk}$.

At the galactic scale, *stars* act as "atoms" whose binding energy shapes the galaxy; at the extragalactic scale, *galaxies* in turn become the "atoms" of the medium, and their distribution governs ΔE_p.

Treatment of Galactic Gas

The crucial point, in the context of General Relativity in the weak-field regime, is that the gravitational potential energy at a given smoothing scale ℓ depends only on the smoothed baryonic density field $\rho^{(\ell)}(\mathbf{x})$, and not on the microscopic nature (stars vs. gas), provided the gas remains non-relativistic ($p \ll \rho c^2$). In other words, if we compare two components of equal mass M that share the same density geometry at scale ℓ (i.e., same smoothed profile and same isodensity surfaces), then their potential energy per unit mass is identical:

$$\frac{\Delta E_{p,g}^{(\ell)}}{M_g^2} = \frac{\Delta E_{p,\star}^{(\ell)}}{M_\star^2} \quad \text{as soon as} \quad \rho_g^{(\ell)}(\mathbf{x}) \propto \rho_\star^{(\ell)}(\mathbf{x})$$

In this sense, for equal mass and identical smoothed density fields, the gas "possesses" the same potential energy as the stellar clumps. Composition does not enter into the gravitational source at this level of approximation.

Practical Consequences.

- **Shape projection at fixed ℓ.** If we adopt a smoothing scale $\ell_{\rm gal}$ (kpc) and project the gas onto the same smoothed spatial shape as the dominant stellar distribution $\rho_\star^{(\ell_{\rm gal})}$ (or, failing that, onto a family of profiles with fixed shape), then $\Delta E_{p,g}^{(\ell_{\rm gal})}$ per unit mass coincides with that of the stars. In hierarchical calculations, the gas can thus contribute to the same stellar probability density function, without additional correction.

- **More diffuse gas (different clumping).** If the gas is less concentrated than the stars at scale ℓ (i.e., has a clumping factor closer to 1), then $|\Delta E_{p,g}^{(\ell)}|$ is slightly smaller for comparable mass and effective radius. A simple multiplicative correction consists in introducing a factor $f_{\rm clump}(\ell) \in [1, \sqrt{C_g}]$ (with $C_g = \langle \rho_g^2 \rangle / \langle \rho_g \rangle^2$) to bring the gas energy closer to that of a component with stellar-like shape.

- **Pressure and multiphase structure.** Gas pressure only weakly affects the active mass in this regime ($(\rho c^2 + 3p)/c^2 \simeq \rho$); it governs the equilibrium state (hydrostatic, turbulent, multiphase) but does not challenge the equality above, to within a few percent.

In summary — for calculations at ℓ_{gal}, we have adopted only the following minimal assumption to treat the gas as a baryonic mass that, for equal mass and smoothed shape, contributes equally to the potential energy as stellar clumps. This simple closure yields empirically satisfactory results for the sample under consideration. Ideally, with more detailed data (separate gas/star profiles, thicknesses, turbulence constraints), the approach could be refined; discrepancies appear only if the smoothed shape (and thus the effective density) differs, which we correct via an explicit clumping factor $f_{\text{clump}}(\ell)$.

Theoretical Models

We apply our gravitational potential energy theory to generate theoretical models in the form of curves, representing the dark mass ratio produced by galaxies with varying numbers of stars. Each curve corresponds to a different galaxy size (Figures 1a and 1b).

The x-axis represents the stellar mass M_S, expressed in solar masses, of the stars of the galaxy. Stellar radii are determined using the standard mass-radius relationship for main-sequence stars ($R \propto M^{0.8}$ if $M < M_\odot$, $R \propto M^{0.57}$ otherwise). The y-axis shows the ratio of total gravitationally induced dark mass M_G to the total baryonic stellar mass M_B, that is, M_G/M_B.

For example, a galaxy with 100 billion stars (thin dotted line) yields a dark mass ratio of approximately 28 when all the stars have $1\,M_\odot$ and $1\,R_\odot$. A population of 200 billion stars yields a ratio of 45, and 300 billion stars results in a ratio of 60. These values exceed the commonly accepted ratio of around 20 for the Milky Way.

Nevertheless, the order of magnitude is consistent, despite the extreme simplification of this analysis. This result reinforces the central hypothesis that dark mass is not a distinct form of matter but rather emerges from the gravitational potential energy of the system.

Impact of Stellar Density Variations on Dark Mass Production

The inclusion of less dense stars, such as red giants, significantly reduces the modeled production of gravitationally induced dark mass (Figures 2a and 2b). This scenario is based on the same stellar population used in previous cases, composed primarily of stars with $1\,M_\odot$ and $1\,R_\odot$, to which a variable fraction of red giants is added, each with $4\,M_\odot$ and $100\,R_\odot$. The resulting decrease in average stellar density lowers the total gravitational potential energy of the system and, consequently, the dark mass ratio.

Conversely, the addition of dense stellar remnants, such as white dwarfs ($0.6\,M_\odot$, $0.0085\,R_\odot$) and neutron stars ($1.35\,M_\odot$, 10.8 km), leads to a dramatic increase in dark mass production (Figures 3a and 3b). The extremely high densities of these objects substantially elevate the system's total potential energy. In realistic stellar populations, however, this increase is moderated by the presence of low-density stars (e.g., red giants).

Figure 1: Dark mass production from main-sequence stellar populations for 10–90 and 100–900 billion stars.

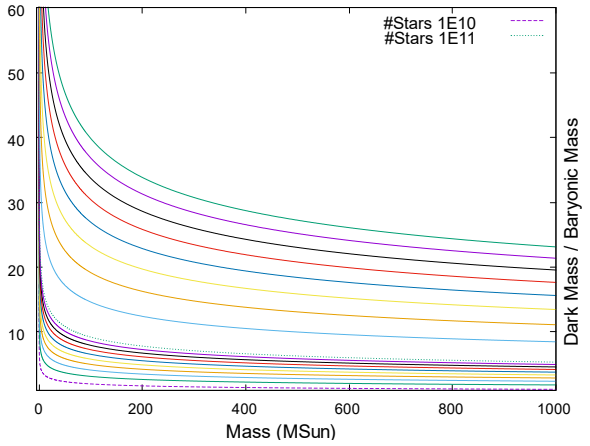

(a) Dark mass ratio for 0–1000 $M_{\odot}$.

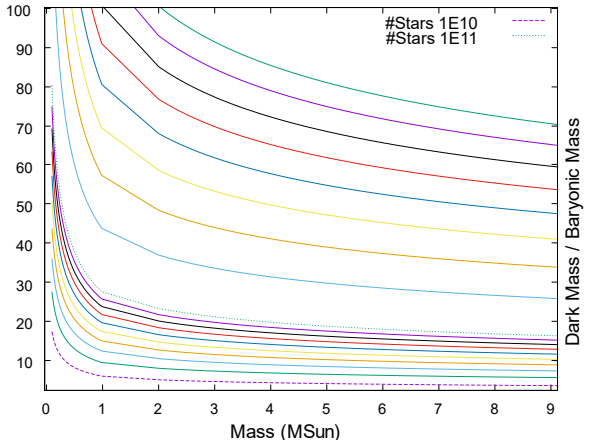

(b) Dark mass ratio for 0–9 $M_{\odot}$.

Figure 2: Impact of red giants on gravitational potential energy for 10–90 and 100–900 billion stars.

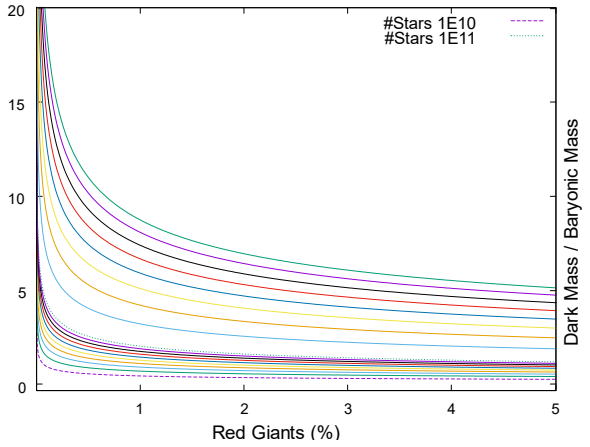

(a) Dark mass ratio for 0%–5% of red giants.

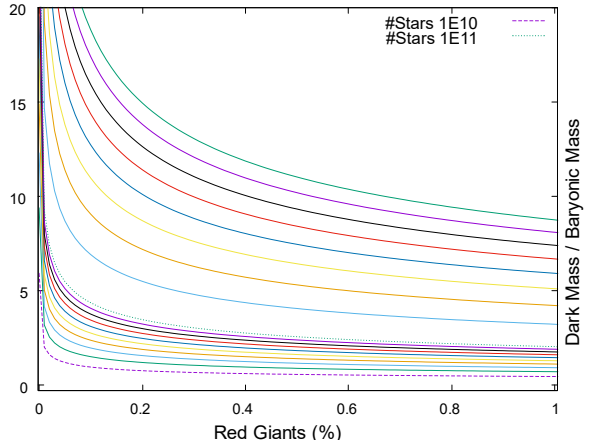

(b) Dark mass ratio for 0%–1% of red giants.

Figure 3: Contribution of compact stellar remnants to gravitational potential energy for 10–90 and 100–900 billion stars.

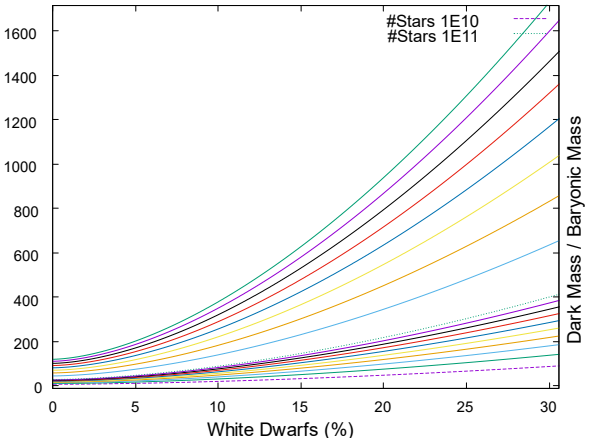

(a) Dark mass ratio for 0%–30% of white dwarfs.

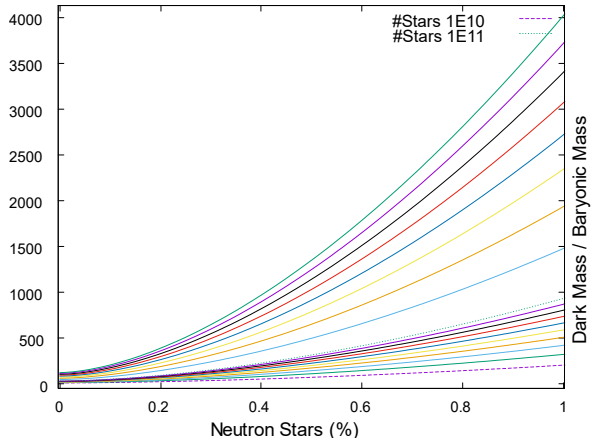

(b) Dark mass ratio for 0%–1% of neutron stars.

Black Holes

Although the gravitational potential energy of stellar systems can now be calculated using the methods described earlier, extending the analysis to black holes introduces additional complexity. However, the underlying principle remains the same: gravitational potential energy is defined as the difference between two configurations—the initial merged black hole and the final state consisting of two separate black holes.

As in the stellar case, the relevant quantity is the energy released during the merger. According to general relativity (see references [15, 16]), the final mass M_f of the remnant black hole is given by:

$$M_f = (M + m)\,(1 - \eta\,\varepsilon_{\text{rad}}(q, \chi))$$

where:

$$\eta = \frac{Mm}{(M+m)^2}, \quad q = \frac{m}{M} \leq 1, \quad \chi = \text{spin parameter}$$

and $\varepsilon_{\text{rad}}(q, \chi)$ is an empirical function representing the efficiency of gravitational wave emission. For non-spinning black holes, a commonly used approximation is:

$$\varepsilon_{\text{rad}}(q) = 0.048 \cdot \frac{(1-q)^2}{(1+q)^4}$$

The effective spin of the remnant is given by:

$$\chi_{\text{eff}} = \frac{M\chi_M + m\chi_m}{M+m}$$

If the spins are randomly oriented, the net spin tends to average to zero, i.e., $\chi_{\text{eff}} \approx 0$.

Let $f(m, M) \to M_f$ be a function representing the final mass of a black hole formed by the merger of two black holes of mass m and M, using the relativistic formula above.

To generalize to n black holes, we reduce to the case of n identical black holes of mass m, so the total initial mass is $M = nm$. Define a recursive function $g(n, m) \to M_f$, where $g(n, m)$ returns the final mass after merging n black holes of mass m:

Algorithm

$$g(n,m) \to \left\{ \begin{array}{lll} \text{if } n = 2 & \Rightarrow & M_f{=}f(m,m) \\ \text{if } n = 3 & \Rightarrow & M_f{=}f(m,m),\ M_f{=}f(m,M_f) \\ \text{else} & & \\ \quad \text{if odd}(n) & \Rightarrow & n = n-1,\ \text{flag odd} \\ \quad M_f{=}g(n/2,m) & & \\ \quad M_f{=}f(M_f,M_f) & & \\ \quad \text{if flag odd} & \Rightarrow & M_f{=}f(m,M_f) \end{array} \right\} \to M_f$$

This recursive structure is particularly suited to dynamic programming. By storing intermediate results of $g(a, b)$ in a memoization table, the total number of distinct calculations is reduced, achieving logarithmic complexity in the number of mergers, i.e., $O(\log_2 n)$.

Negligible Contribution to Gravitational Potential Energy

The gravitational potential energy produced by black hole mergers is extremely limited, as it directly derives from the initial mass. By definition, the radiated energy—mainly in the form of gravitational waves—can never exceed the total mass–energy of the system.

Even in ideal conditions (e.g., prograde aligned spin configurations), the fraction of mass converted to gravitational wave energy remains small. Using a semi-analytic approximation from numerical simulations [17, 18], the radiated fraction is:

$$\frac{E_{\text{gw}}}{M} \approx \eta(1 - 4\eta)\left[1 - 0.0686(1 - \chi_{\text{eff}})^2\right]$$

In the most favorable scenario—mergers involving black holes with masses greater than $500\,M_\odot$ with spins close to unity—the maximum energy fraction remains below 16%.

Given this upper limit and the relatively low abundance of black holes in most galactic environments, their contribution to the total gravitational potential energy by fusion is negligible.

The Volume Conservation Issue

Despite their low contribution by fusion, black holes must be included in gravitational energy calculations. According to Newtonian gravity, any massive object contributes via:

$$E_p = -\frac{GmM}{d}$$

Consider building the theoretical compact configuration that conserves the total volume of stars, yielding a body of mass M and volume V. If the system also contains n black holes of mass m and volume v, the revised mass and volume are $M' = M + nm$, $V' = V + nv$.

However, black hole mergers reduce total volume, unlike stars. Including them in the compact configuration breaks the volume conservation hypothesis and introduces a conceptual inconsistency.

This highlights a unique property of black holes; they violate volume conservation through fusion. Though they must be included in potential energy calculations, their geometric behavior challenges the core assumption of volume preservation.

Limiting Case of Gravitational Potential Energy

This suggests that black holes should be treated analogously to ordinary matter within a volume-preserving compact configuration — but with the caveat that their peculiar volumetric behavior must be respected.

However, any attempt of this kind would either increase the system's energy or absorb the surrounding potential energy. Indeed, the outcome can appear dense (e.g., $\rho \sim 1000$ for $4.3 \times 10^6\, M_\odot$) or extremely diffuse (e.g., $\rho \sim 0.001$ for $4.3 \times 10^9\, M_\odot$), owing to the nonlinear scaling of the Schwarzschild radius with mass.

As the system approaches a single black hole, the "no-hair" theorem implies that internal structure is erased — no resolved mass distribution, no self-gravitational interaction, and thus no potential energy in the classical Newtonian sense. Black holes are the endpoint of gravitational compaction. As their dominance increases, the accessible gravitational binding potential energy inevitably decreases.

All of this implies that, to respect energy conservation and the "no-hair" principle, the only consistent way to treat the potential energy of black holes is to assign them none. This is also the only empirical choice that yields excellent observational agreement.

Galactic Models

In order to assess whether gravitational potential energy alone can explain the dark mass observed in galaxies, we tested our theoretical model against the SPARC sample [20], which includes rotation curve data for 175 galaxies as well as the mass models of each. For each data point, the set provides the observed velocity V_{obs}, the contribution of the baryonic mass contained within the orbital radius V_{bar}, as well as its decomposition into bulge stars (V_{bul}), disk stars (V_{disk}), and gas (V_{gas}). These values are used to estimate the mass contained within the orbital radius ($M_{\text{bul}}, M_{\text{disk}}, M_{\text{gas}}$) from the mass models. The required dark mass M_{dark} is then computed by comparing the observed acceleration with that predicted by the visible matter. Each point also includes an estimate of the uncertainty eM_{dark} associated with the inferred dark mass.

This dataset contains 3,386 kinematic data points, of which 3,048 (90 %) were retained for analysis. Data points with negative dark mass values or negative errors were discarded in order to ensure consistency and reliability. The galaxy F574-2 was entirely excluded because it did not contain any valid data points.

Description of the Algorithm

For each galaxy G, our optimization algorithm $f(G, \rho, P, k\sigma)$ uses a fixed ρ vector of stellar densities and stellar proportions $P \pm k\sigma$ to calculate E_{dark} (the potential energy) of each data point $(M_{\text{bar}}, M_{\text{dark}}, eM_{\text{dark}})$, with:

$$M_{\text{bar}} = M_{\text{bul}} + M_{\text{disk}} + M_{\text{gas}}.$$

The treatment of gas assumes a complete smoothing of its potential energy by the stellar distribution.

The calculation of E_{dark} results from the algorithm previously described (see « practical estimation from a stellar histogram »). For each point, the error is given by:

$$\Delta_{\text{dark}} = |E_{\text{dark}} - M_{\text{dark}}|.$$

A point is considered solved if $\Delta_{\text{dark}} < 2eM_{\text{dark}}$, that is, if the error bars overlap. Although a more precise approach should include both the uncertainty on M_{dark} and that on the prediction E_{dark}, we consider eM_{dark} as the effective error margin, for practical simplification.

The algorithm first searches for a point it can solve. To do this, it slightly modifies the distribution P in order to minimize Δ_{dark} at each step (greedy method). The resulting distribution P' must always satisfy $P \pm k\sigma$. In case of failure, the algorithm retries with another distribution including an additional gas clumping component. If it still fails, no point of the galaxy is solved.

Then, the algorithm attempts to solve the neighboring points of the first successful point, using P', under the assumption that nearby points should have similar distributions. It propagates the solution step by step. If a point fails, it moves on to the next one. A galaxy whose all points are solved is considered solved.

Initial Population

We use as initial population a distribution composed of black holes (BH), neutron stars (NS), white dwarfs (WD), red giants (RG), as well as the usual spectral classes of the main sequence M, K, G, F, A, B and O. This choice is based on the statistical representativeness in mass and on the variability of density, the only factor influencing the production of dark mass.

In the nearby Universe ($z \approx 0$), as recorded in SPARC, a set of average mass fractions, normalized to 1, can be written:

$\mathrm{BH} = 1.0\% \pm 0.5\%$	$\mathrm{NS} = 0.3\% \pm 0.1\%$	$\mathrm{WD} = 2.2\% \pm 0.7\%$
$\mathrm{RG} = 0.2\% \pm 0.1\%$	$\mathrm{M} = 55\% \pm 10\%$	$\mathrm{K} = 16\% \pm 6\%$
$\mathrm{G} = 10.5\% \pm 5\%$	$\mathrm{F} = 5.5\% \pm 3\%$	$\mathrm{A} = 5\% \pm 2\%$
$\mathrm{B} = 3\% \pm 1\%$	$\mathrm{O} = 1.3\% \pm 0.5\%$	

With the following usual mean densities ($\mathrm{kg/m^3}$):

$\rho_{\mathrm{NS}} = 4 \times 10^{17}$	$\rho_{\mathrm{WD}} = 1 \times 10^{9}$	$\rho_{\mathrm{RG}} = 5 \times 10^{-4}$
$\rho_{\mathrm{M}} = 9 \times 10^{3}$	$\rho_{\mathrm{K}} = 2.4 \times 10^{3}$	$\rho_{\mathrm{G}} = 1.41 \times 10^{3}$
$\rho_{\mathrm{F}} = 1.06 \times 10^{3}$	$\rho_{\mathrm{A}} = 29$	$\rho_{\mathrm{B}} = 6.3$
$\rho_{\mathrm{O}} = 5.2$		

These stellar mass distributions correspond to an instantaneous snapshot of the populations observed in local galaxies. Empirical surveys of the nearby field, in particular those from SDSS [21] and catalogs of white dwarfs [22], show that stellar mass is dominated by low-mass stars (M, K, and G dwarfs), while compact remnants (WD, NS, BH) represent only a minor fraction, of the order of a few percent in total. In the Milky Way, M dwarfs account for more than half of the stellar mass of the disk, and the local fractions in white dwarfs ($\sim$2–3%), neutron stars ($\sim$0.1–0.3%), and stellar black holes ($\sim$0.5–1%) are all consistent with direct measurements. The fraction in red giants remains low ($\sim$0.1–0.5%), in agreement with the shortness of this evolutionary phase. This configuration – strong dominance of M/K/G dwarfs and limited compact remnants – corresponds precisely to the distribution adopted for SPARC.

The second distribution uses the same proportions but adds a gas aggregation component with a density $\rho_{\mathrm{GC}} = 1.3 \times 10^{-18}$, corresponding to the mean density of cold gas. To establish the initial proportions, we ran our algorithm to solve the sub-population not resolved by the first distribution, then we iteratively reused as starting distribution the average distribution of the resolved points. This algorithm converged to the following initial population:

$\mathrm{BH} = 0.76\% \pm 0.5\%$	$\mathrm{NS} = 0.25\% \pm 0.1\%$	$\mathrm{WD} = 2.1\% \pm 0.7\%$
$\mathrm{RG} = 0.11\% \pm 0.1\%$	$\mathrm{M} = 67\% \pm 10\%$	$\mathrm{K} = 16\% \pm 6\%$
$\mathrm{G} = 4.8\% \pm 5\%$	$\mathrm{F} = 3.7\% \pm 3\%$	$\mathrm{A} = 3.1\% \pm 2\%$
$\mathrm{B} = 1.6\% \pm 1\%$	$\mathrm{O} = 0.78\% \pm 0.5\%$	$\mathrm{GC} = 1.02 \times 10^{-13} \pm 1 \times 10^{-13}$

The « clumping » factor being simply an empirical adjustment factor, these values remain plausible for a late-type disk population of the « bottom-heavy » kind. Which is indeed the case for a significant portion of the galaxies used to create this distribution.

Model Fitting Results

The model shows an excellent agreement with the observational data; this agreement varies with the factor k ($P \pm k\sigma$). Here are the results (Table 3) using only the first stellar distribution and adding the second.

Table 3: Comparison of resolution as a function of k factor.

	First Distribution		With Second Distribution	
k	**Points Solved**	**Galaxies Solved**	**Points Solved**	**Galaxies Solved**
1σ	800 (26.3%)	24 (13.8%)	1,086 (35.6%)	31 (17.8%)
2σ	1,375 (45.1%)	77 (44.3%)	2,935 (96.3%)	145 (83.3%)
3σ	1,999 (65.6%)	105 (60.4%)	3,001 (98.5%)	158 (90.8%)
4σ	2,069 (67.9%)	109 (62.6%)	3,005 (98.6%)	162 (93.1%)
5σ	2,133 (70.0%)	113 (64.9%)	3,020 (99.1%)	163 (93.7%)

Thus, with a 3σ distribution, our algorithm solves more than 98 % of the data points and 90 % of the galaxies. This unambiguously confirms that gravitational potential energy, generated by the expected distribution of stars, can explain galactic dark mass.

The sub-population solved by the first distribution at 3σ (105 galaxies) is composed mostly of galaxies of types Scd / Sd / Sdm / Sm / Im / BCD, with a few Sbc / Sc (with one Sa and one Sb). The mean gas concentration is 66% with $M/L = 1.9$ and a disk extent of 2.1. The ratio of dark to baryonic mass is 4.6. In this type of galaxy, the gas is diffuse and the smooth hypothesis (without clumping) is fully justifiable.

The sub-population solved by the second distribution at 3σ (59 galaxies) is composed of galaxies of types S0 / Sa / Sab / Sb / Sbc / Sc / Scd, and overlaps with the first population only through types Sbc / Sc / Scd. The mean gas concentration is 24% with $M/L = 0.80$ and a disk extent of 4.9. The ratio of dark to baryonic mass is 3.3. These are typically intermediate spiral galaxies with extended disks. The low gas concentration explains the success of adding a simple clumping factor.

The last sub-population not solved at 3σ (16 galaxies) is composed mostly of galaxies of types Sm / Im / BCD (with one Sdm, one Scd and one Sab). It therefore lies at the opposite side of the spectrum from the types solved by the second distribution, namely irregular galaxies. The mean gas concentration is 72% with $M/L = 5.3$ and a disk extent of 1.9. The ratio of dark to baryonic mass is 7.1. These are typically late-type irregular / dwarf galaxies very rich in gas. In this type of galaxy, the gas is multiphase and clumpy (GMC, CNM) and at very high concentration, which complicates the adjustment of the clumping factor.

The previous analysis highlights the sensitivity and specificity of our algorithm. Although it is possible that different stellar distributions may lead to similar results, the imposed constraints appear to be strong. The distribution capable of correctly reproducing the observed dark mass must therefore remain close to the actual stellar distribution. Some classes of stars with comparable density can be interchanged, but the proportions between classes of markedly different density must be preserved. Moreover, the algorithm tends to favor globally consistent proportions, since the best solution obtained at a given point is transmitted to its neighbors. Figure 4 illustrates the agreement between the generated potential energy and the expected dark mass, while Figure 5 shows the stellar distribution required for this agreement.

Figure 4: Example (galaxy UGC 2953) of the generated potential energy and the agreement with the experimental error. The mass axis scale is not linear near the origin, the first point corresponds to 8×10^{38} kg.

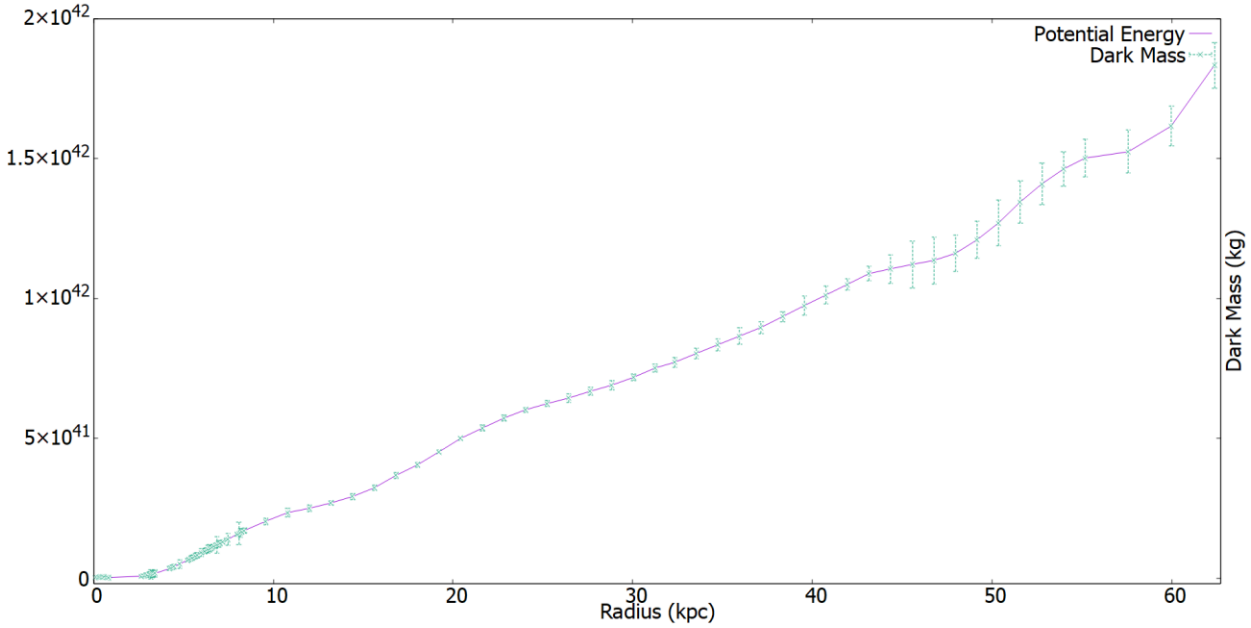

Figure 5: Example (galaxy UGC 2953) of the stellar distribution used to generate the potential energy. We see here the very clear variation of the population in the bulge and the dominance (more than 80%) of the M class.

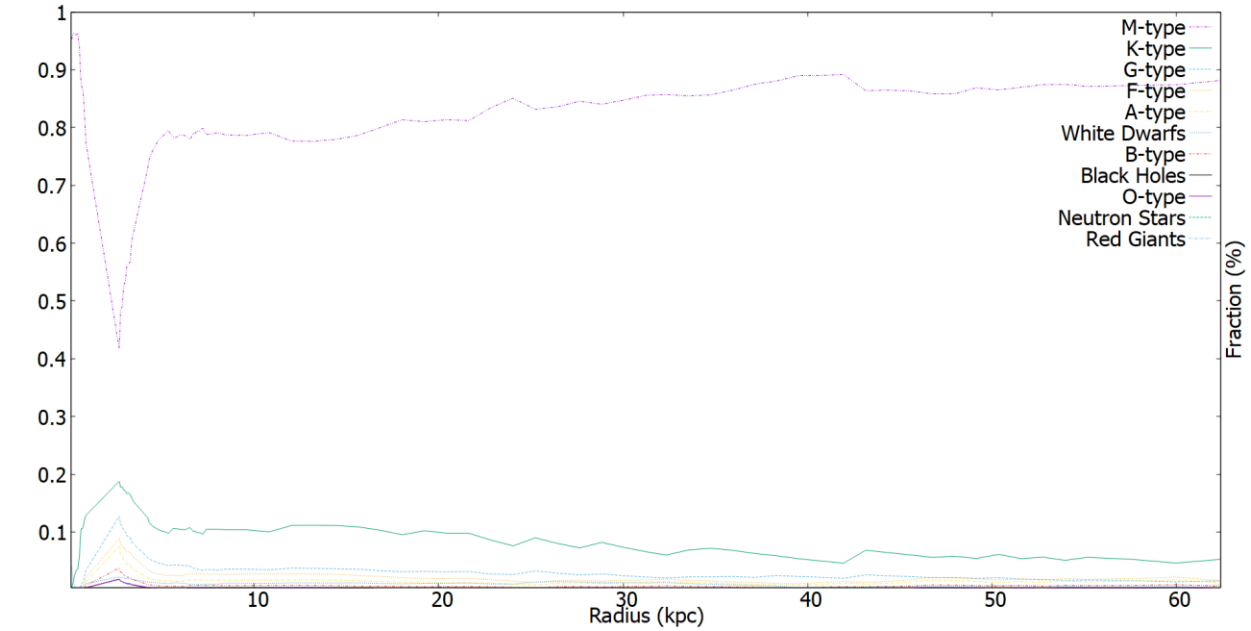

Margin of Error

Although we have demonstrated that a "natural" population of stars does indeed produce the expected potential energy, there is no guarantee that this is not merely a random phenomenon. The algorithm could just as well perform successfully with any fictitious galaxy population that does not conform to observational reality, or even with stellar distributions or densities that are radically different.

In formal logic, we can state that we have shown that the fact that potential energy produces dark mass constitutes a sufficient condition, that is:

Potential energy produces dark mass
$\rightarrow$
Potential energy explains galactic dark mass

The evidence against chance far exceeds 5σ. Indeed, if the success of a single point were due to chance with probability p_0, then the probability that a galaxy with m points is entirely resolved is $\Pr(\text{resolved galaxy}) = p_0^m$. Even under an extremely favorable assumption $p_0 = 0.5$, for $m = 10$ we obtain $p_0^{10} = 0.5^{10} \approx 10^{-3}$, i.e., negligible fractions of resolved galaxies, nowhere near our observations ($> 90\%$ of galaxies and $> 98\%$ of points resolved). Even considering only the first stellar distribution, we already reach 60% of galaxies and 66% of points resolved, which remains incompatible with any reasonable random mechanism (one would then need p_0 close to 1 to raise p_0^m to 0.6 as soon as $m \geq 2$). These orders of magnitude make the chance hypothesis highly implausible, well beyond the usual 5σ threshold. However, we have not shown that this relation constitutes a necessary condition, namely:

Potential energy explains galactic dark mass
$\rightarrow$
Potential energy produces dark mass

In other words, we have an explanatory hypothesis for phenomenological reality; however, we do not have a demonstration that this hypothesis is necessary. Thus, if the world were different, our hypothesis might still successfully explain this "alternate world." What we aim for is that the hypothesis be finely tuned to observational reality: if reality changes, the hypothesis must also evolve.

In our case, what we refer to as "our world" corresponds to the SPARC data as well as to the initial stellar density and distribution vectors confirmed either by observation or by theories that are themselves empirically validated. Therefore, we will focus exclusively on the behavior of the algorithm at 3σ, resolving 105 galaxies and 1,999 data points.

Table 4: Z-scores across all galaxies versus scaling factor k. A galaxy is deemed resolved if all its points are resolved. The comparison $k = 1$ vs $k \neq 1$ is performed with McNemar's test (one-sided), and we report the corresponding z-score. To avoid pseudoreplication and to decluster at the galaxy level, we summarize each galaxy by its rate of resolved points $r_g(k)$, then test the paired contrast $d_g(k) = r_g(1) - r_g(k)$ using the *Wilcoxon signed-rank* test (one-sided). The associated z-score is reported for each k.

Factor k	**Baryonic Mass**						**Dark Mass**					
	Galaxies			**Points**			**Galaxies**			**Points**		
	#	%	z	#	%	z	#	%	z	#	%	z
1.0×10^{-12}	6	3.4%	9.8	309	10.1%	10.5	0	0.0%	10.1	0	0.0%	11.5
1.0×10^{-6}	6	3.4%	9.8	309	10.1%	10.5	0	0.0%	10.1	0	0.0%	11.5
1.0×10^{-3}	6	3.4%	9.8	315	10.3%	10.5	1	0.6%	10.1	38	1.2%	11.3
2.5×10^{-3}	6	3.4%	9.8	332	10.9%	10.5	2	1.1%	10.0	91	3.0%	11.2
5.0×10^{-3}	6	3.4%	9.8	361	11.8%	10.3	3	1.7%	9.8	182	6.0%	11.0
7.5×10^{-3}	7	4.0%	9.7	393	12.9%	10.2	8	4.6%	9.3	276	9.1%	10.8
1.0×10^{-2}	7	4.0%	9.7	428	14.0%	10.1	12	6.9%	9.0	358	11.7%	10.6
2.5×10^{-2}	12	6.9%	9.0	855	28.1%	8.3	29	16.7%	7.6	659	21.6%	9.8
5.0×10^{-2}	33	19.0%	6.3	1,446	47.4%	5.5	42	24.1%	6.7	929	30.5%	8.9
7.5×10^{-2}	51	29.3%	4.6	1,705	55.9%	4.4	62	35.6%	5.0	1,093	35.9%	8.0
1.0×10^{-1}	61	35.1%	3.7	1,861	61.1%	3.7	73	42.0%	4.1	1,221	40.1%	7.2
2.5×10^{-1}	90	51.7%	1.4	2,377	78.0%	0.3	102	58.6%	0.4	1,521	49.9%	5.4
5.0×10^{-1}	95	54.6%	1.2	2,445	80.2%	(2.1)	107	61.5%	(0.2)	1,709	56.1%	4.6
7.5×10^{-1}	99	56.9%	1.2	2,233	73.3%	(3.4)	107	61.5%	(0.4)	1,863	61.1%	3.9
1.25	104	59.8%	-	1,826	59.9%	4.5	104	59.8%	-	2,103	69.0%	(3.6)
1.75	106	60.9%	-	1,650	54.1%	4.9	98	56.3%	1.3	2,272	74.5%	(3.5)
2.5	98	56.3%	1.1	1,484	48.7%	5.7	95	54.6%	1.4	2,385	78.2%	(2.4)
5.0	57	32.8%	5.5	1,052	34.5%	8.2	100	57.5%	0.5	2,500	82.0%	(1.4)
7.5	35	20.1%	7.2	783	25.7%	9.5	97	55.7%	0.7	2,445	80.2%	(0.4)
1.0×10^{1}	25	14.4%	7.9	601	19.7%	9.9	91	52.3%	1.3	2,382	78.1%	0.2
2.5×10^{1}	3	1.7%	9.8	170	5.6%	11.0	74	42.5%	2.6	2,060	67.6%	2.6
5.0×10^{1}	1	0.6%	10.1	52	1.7%	11.3	60	34.5%	3.7	1,842	60.4%	3.8
7.5×10^{1}	1	0.6%	10.1	30	1.0%	11.4	51	29.3%	4.6	1,705	55.9%	4.4
1.0×10^{2}	0	0.0%	10.1	23	0.8%	11.4	41	23.6%	5.5	1,591	52.2%	4.9
2.5×10^{2}	0	0.0%	10.1	10	0.3%	11.5	21	12.1%	7.8	1,157	38.0%	6.8
5.0×10^{2}	0	0.0%	10.1	4	0.1%	11.5	10	5.7%	9.3	824	27.0%	8.6
7.5×10^{2}	0	0.0%	10.1	3	0.1%	11.5	9	5.2%	9.4	676	22.2%	9.2
1.0×10^{3}	0	0.0%	10.1	3	0.1%	11.5	7	4.0%	9.7	574	18.8%	9.5
1.0×10^{6}	0	0.0%	10.1	0	0.0%	11.5	6	3.4%	9.8	310	10.2%	10.5
1.0×10^{12}	0	0.0%	10.1	0	0.0%	11.5	6	3.4%	9.8	309	10.1%	10.5

Performance Analysis

We aim to test the robustness of the model without altering its internal constraint space. In particular, stellar densities and stellar proportions define the algorithm's choice space; changing them (to be more lax or more stringent) would amount to *changing the task* and would bias the stress test. We therefore leave them unchanged.

We apply exogenous perturbations to our galaxies. Let a catalog:

$$\mathcal{G} = \left\{ \left(M_{\text{bar}}^{(g)},\ M_{\text{dark}}^{(g)} \pm e_{\text{dark}}^{(g)} \right) \right\}_g$$

For a factor $k > 0$, we consider two transformed datasets for each galaxy g:

$$\text{(i)}\ \ k \cdot M_{\text{bar}}^{(g)} \qquad \text{and} \qquad \text{(ii)}\ \ k \cdot M_{\text{dark}}^{(g)} \pm k \cdot e_{\text{dark}}^{(g)}$$

We explore a grid of values of k spanning several orders of magnitude and compute the z-scores for galaxies solved and resolved points, relative to the unaltered configuration ($k = 1$). The analysis is conducted separately for (i) baryonic mass scaling only and (ii) dark mass scaling only. The corresponding results are reported in Table 4.

Experimental Confirmation

These results are highly significant and unambiguously show maximal resolution efficiency near $k \simeq 1$. The z-score increases on both sides of 1 as soon as we move away from it.

Galaxy level: the baryonic mass shows a clear increase in z from $k \geq 5$ ($z \geq 5.5$) and from $k \leq 0.1$ ($z \geq 3.7$). The dark mass exhibits the same bilateral behavior, starting from $k \geq 25$ ($z \geq 2.6$) and from $k \leq 0.1$ ($z \geq 4.1$).

Point level: the baryonic mass shows an increase in z from $k \geq 1.25$ ($z \geq 4.5$) and from $k \leq 0.1$ ($z \geq 3.7$). The dark mass shows an increase in z from $k \geq 25$ ($z \geq 2.6$) and from $k \leq 0.75$ ($z \geq 3.9$). Taken together, these thresholds define a robust tolerance interval $k \in [0.75, 1.25]$ so $k = 1.0 \pm 0.25$ at almost 4σ. Indeed, a natural combined rule is to multiply the baryonic and dark masses when $k > 1$ and $k < 1$, respectively.

The probability that the mantissa (1.0), contradicting the null hypothesis, falls exactly within this interval is $1/20 = 5\%$. Moreover, given the usual baryonic and dark masses ($\gtrsim 10^{30}$ kg), the null hypothesis, remaining conservative, could very well have been verified for an exponent of ± 10, i.e., another $1/20$, for a combined total of $1/400 = 0.25\%$.

However, this is not a statistical phenomenon of the type "a value falls into a numerical interval." The evidence comes from the functional profile $z(k)$ under plausible alternative worlds: (1) $z(k)$ could be flat (no dependence on k); (2) show only weak undulations with no peak near $k = 1$; or (3) reach its optimum far from $k = 1$. Our data show the opposite: a bilateral increase of $z(k)$ as $|\log k|$ grows, with a peak near $z(k \simeq 1)$. It is difficult to assign a precise probability to the contradiction of the null hypothesis here, but granting another 5% is conservative. Altogether, this yields a combined total of $1/8000$, i.e., more than 3.5 σ.

These results provide experimental confirmation that the model identifies $k \simeq 1$ as the physical regime, and that any marked scaling (above or below) systematically degrades the resolution. They thus corroborate the potential-energy explanation of the phenomenon of galactic dark mass.

Galactic Dark Mass in the Cosmological Framework

The previous section showed that our model of dark mass (gravitational binding energy) can faithfully reproduce individual galactic data from the SPARC sample. It is therefore natural to extend this approach to the entire Universe, applying the same principles of stellar potential energy calculation, but this time through a synthetic population of galaxies covering the space of galactic masses and densities. The objective being to reproduce an important factor of ΛCDM cosmology (Table 5), namely the total galactic dark mass.

Table 5: ΛCDM mass budget ($z \approx 0$) for the observable Universe. Absolute values and fractions are derived from the Planck 2018 parameters (Ω_m, Ω_b, H_0) setting $\rho_{\mathrm{crit},0}$ and M_{tot}, then from a "galactic" (within halos) / "extra-halo" partition obtained from large simulations (Illustris/TNG/EAGLE). The 1 σ uncertainties reflect only cosmological errors; systematics due to the definition of halos and feedback are not included.

ΛCDM Values			
	Description	**Value $\pm 1\ \sigma$ (kg)**	**Fraction $\pm 1\ \sigma$**
M_{gbar}	Galactic baryonic mass	$(3.196 \pm 0.122) \times 10^{52}$	$3.33\% \pm 0.13\%$
M_{gdark}	Galactic dark mass	$(4.075 \pm 0.111) \times 10^{53}$	$42.51\% \pm 1.16\%$
M_{ebar}	Extragalactic baryonic mass	$(1.181 \pm 0.045) \times 10^{53}$	$12.32\% \pm 0.47\%$
M_{edark}	Extragalactic dark mass	$(4.010 \pm 0.109) \times 10^{53}$	$41.84\% \pm 1.14\%$
M_{tot}	Total mass	$(9.586 \pm 0.256) \times 10^{53}$	$100.00\% \pm 2.67\%$

To achieve this objective, we developed a program that generates galaxies according to a two-dimensional grid of baryonic mass–mean density. Each synthetic galaxy is described by a total baryonic mass and a mean density ρ_{gal}, derived from a disk geometry (effective radius and scale height) where the gas is considered fully smoothed by the stellar distribution. The stellar content is based on the same fixed density vector ρ as in the previous section, including the spectral classes O–M and the compact remnants (black holes, white dwarfs, neutron stars, and red giants). However, we use the following average stellar population, where only the stars with large density variability (BH, NS, WD, RG) have explicit uncertainty bounds to create the lower and upper envelopes of potential energy. The main-sequence classes (O–M) adjust in proportion so as to preserve the normalization of the stellar population :

$\mathrm{BH} = 0.8\% \pm 0.19\%$	$\mathrm{NS} = 0.64\% \pm 0.15\%$	$\mathrm{WD} = 8.0\% \pm 2.0\%$
$\mathrm{RG} = 1.5\% \pm 0.6\%$	$\mathrm{M} = 13.1\%$	$\mathrm{K} = 13.7\%$
$\mathrm{G} = 6.2\%$	$\mathrm{F} = 6.4\%$	$\mathrm{A} = 7.9\%$
$\mathrm{B} = 27.8\%$	$\mathrm{O} = 14.0\%$	

These stellar mass distributions do not describe a local instantaneous snapshot as for SPARC, but rather a mass-integrated population at $z \approx 0$, consistent with the cosmic star formation history and an IMF of the Chabrier or Kroupa type [23, 24]. Population synthesis models such as BC03, FSPS, Maraston, and BPASS [25, 26, 27, 28, 29, 30], coupled with the cosmic SFH [31], predict that a substantial fraction of the stellar mass formed at high redshift has already evolved into compact remnants by $z = 0$. In this framework, white dwarfs dominate the mass of remnants, while neutron stars and stellar black holes contribute at the per-mille ($\sim$1%) level of the total mass, depending on the IMF and IFMR adopted. The massive progenitor bins (O and B) are then interpreted as categories that represent both the short-lived stars and the cumulative contribution of their compact descendants, which justifies an increased weighting of these components in the integrated pipeline estimate.

Thus, our program simply applies iteratively the function f from the subsection « practical estimation from a stellar histogram » :

$$\left\{\begin{array}{l} \Delta E_p = 0 \\ \textbf{for all } (M_i, N_i) \\ \qquad M_t = R_t = 0 \\ \qquad \textbf{for all } (\rho_j, P_j) \\ \qquad\qquad f(\rho_j, M_i \times P_j, M_t, R_t) \to (\Delta E_{\mathrm{pi}}, M_t, R_t) \\ \qquad\qquad \Delta E_{\mathrm{p}} = \Delta E_{\mathrm{p}} + \Delta E_{\mathrm{pi}} \times N_i \end{array}\right\} \to \Delta E_p$$

For each class i of N_i galaxies of mass M_i, we calculate the total potential energy generated. This is done for the average stellar proportion P_j, as well as for the high and low bounds (maximizing or minimizing the density). This yields 4.28×10^{53} kg $\in [2.77 \times 10^{53}$ kg, 6.06×10^{53} kg].

The agreement with the ΛCDM value is striking, namely 4.28×10^{53} compared to 4.08×10^{53}. The ΛCDM error margin is so small compared to ours that we may treat this value as point-like. The probability that the mantissa (4.08), contradicting the null hypothesis, falls exactly within this interval is 32%. Moreover, remaining conservative, the null hypothesis could very well have been verified for an exponent of ± 10, i.e. another 5%, giving a combined total of 1.6%.

This constitutes an independent demonstration from SPARC that potential energy and dark mass are one and the same phenomenon. Indeed, the proportion values used here are completely different and no adjustment mechanism is performed. In addition, the scale is different since we sum over all the galaxies in the Universe. The cumulative probability is $1/8,000 \times 1.6\% = 1/500,000$, corresponding to approximately 4.75 σ. Let us note that by being slightly more lax and taking an exponent margin of ± 12, we already exceed 5 σ confidence.

Extragalactic Dark Mass and Newtonian Limits

The application of Newtonian dynamics at the scale of individual galaxies remains valid insofar as the characteristic velocities remain small and cosmological expansion does not

compromise classical gravitational binding. A galaxy, or even a small group of galaxies, can thus be satisfactorily described by the law of universal gravitation, without the dilation of space intervening in any measurable way. This local validity highlights the robust character of the Newtonian approximation in weak-field regimes, as long as the size of the systems remains limited.

However, beyond a radius of the order of ~ 10 Mpc, the situation changes fundamentally: the expansion of the Universe introduces an effective acceleration that eventually surpasses the Newtonian binding energy between distant galaxies. In relativistic terms, this transition is well captured by the *turnaround radius*, $R_{\rm ta}$, expected in a Schwarzschild–de Sitter (Kottler) framework or, equivalently, in Newtonian spherical collapse with Λ [32, 33]. In ΛCDM, the theoretical maximum bound

$$R_{\rm ta,max} = \left(\frac{3GM}{\Lambda c^2}\right)^{1/3}$$

provides a clear criterion for the effective dynamical reach of a halo's gravity [32].

To set the scales, the *turnaround blocks* (RG) are defined as the maximal volumes within which local gravity still prevails over expansion. Their size and content vary strongly depending on the environment. In the *field* (isolated galaxies), the characteristic size of the block is of order ~ 3 Mpc and it typically contains only a few galaxies (on the order of 1–10). Modest *groups* reach blocks of about ~ 6 Mpc on a side, assembling on average a few dozen galaxies (on the order of 10–40), while *clusters* possess blocks that can exceed ~ 10 Mpc on a side and gather $\sim$ 100–200 galaxies, with rich cases reaching $\sim$ 300–400 and rarer extremes [34, 35]. These scales and abundances are consistent with observed group and cluster catalogs as well as recent theoretical syntheses [35].

We therefore reused our synthetic population at $z = 0$, dividing the Universe of galactic baryonic mass 3.196×10^{52} kg (ΛCDM) into $N = 1.7045 \times 10^{14}$ galaxies. It is then sufficient to divide N into n blocks of size t (in number of galaxies) and to evaluate the potential energy $E_{\rm block}$ generated by one block on average, and then multiply $E_{\rm block}$ by n to recover the ΛCDM value of 4.01×10^{53} kg. However, each of these blocks contains a fraction of the turnaround energy, $E_{\rm turn} = 6 \times 10^{43}$ kg, which we represent by the ratio $E_{\rm block}/E_{\rm turn}$.

The principle is straightforward, since we have already compacted the stars of our galaxies into spheres to produce galactic dark mass, it now suffices to merge these spheres in order to produce extragalactic dark mass within each turnaround cell.

With our algorithm, there is no need to worry about issues such as "computing the energy at the boundaries of the cells" or "ensuring that no double counting occurs." Each merger of galaxies (compact spheres of stellar density) preserves the baryonic mass, and the energy released in the merger must be accounted for. Even though we did not merge galaxies across adjacent cells, the intercellular energy is nonetheless included. Indeed, had we merged galaxies from neighboring cells, on average the number of galaxies per cell would have remained unchanged, and the final state would be identical.

The results (Table 6) show that the interval of the number of galaxies per cell (12–641) required to reproduce the total ΛCDM extragalactic dark mass is very close to the expected

range (1–400). Considering that we have 1.7×10^{14} galaxies in this simulation, the probability of obtaining such an interval purely by chance is less than $\sim 10\,\%$. Furthermore, the total mass of a turnaround block (100%) corresponds to the median value of the table, which is consistent with statistical expectation. Indeed, a real block is composed of a mixture of galaxies of different sizes rather than of a single homogeneous class. The fact that the 100% value lies at the center of the range reflects this median property, with a probability of occurrence by pure chance of less than $\sim 10\,\%$.

Here again, this is an algorithm and a parametrization entirely distinct, based on physical assumptions independent from those used for SPARC and for the estimate of the total galactic dark mass. By remaining very conservative, it is possible to add an additional 1/20 factor to our global error margin, which then becomes $(1/20)^4 \times 1.6\,\% \approx 1/10\,000\,000$, corresponding to $5.4\,\sigma$.

Table 6: Synthetic galactic block sizes (in number of galaxies) required to reproduce the total extragalactic dark mass (ΛCDM), and associated turnaround mass fraction, for the different mass classes at $z = 0$.

Mass Class (kg)	Universe Fraction (%)	Block Size (#)	Turnaround Mass Fract. (%)	Mass Class (kg)	Universe Fraction (%)	Block Size (#)	Turnaround Mass Fract. (%)
9.6×10^{37}	24%	641	2%	1.5×10^{40}	0.73%	84	209%
1.3×10^{38}	17%	560	2%	2.1×10^{40}	0.62%	74	315%
1.9×10^{38}	13%	489	3%	3.0×10^{40}	0.50%	64	466%
2.6×10^{38}	10%	427	4%	4.1×10^{40}	0.38%	56	702%
3.7×10^{38}	7.8%	373	5%	5.8×10^{40}	0.29%	49	1,061%
5.2×10^{38}	6.1%	326	6%	8.1×10^{40}	0.21%	43	1,613%
7.3×10^{38}	4.8%	285	9%	1.1×10^{41}	0.15%	37	2,408%
1.0×10^{39}	3.8%	249	12%	1.6×10^{41}	0.091%	32	3,621%
1.4×10^{39}	3.1%	217	16%	2.2×10^{41}	0.050%	28	5,522%
2.0×10^{39}	2.4%	190	23%	3.1×10^{41}	0.023%	25	8,608%
2.8×10^{39}	2.0%	166	32%	4.4×10^{41}	0.0085%	21	12,613%
3.9×10^{39}	1.6%	145	46%	6.1×10^{41}	0.0021%	19	19,960%
5.5×10^{39}	1.4%	127	66%	8.6×10^{41}	0.0003%	16	29,377%
7.7×10^{39}	1.1%	111	97%	1.2×10^{42}	0.0000%	14	44,980%
1.1×10^{40}	0.9%	97	143%	1.7×10^{42}	0.0000%	12	67,478%

The Gravitational Mass–Energy Field

To understand how gravitational potential energy—interpreted here as dark mass—affects galactic rotation curves, we must first consider the spatial distribution of this mass–energy. Unlike baryonic matter, this invisible component is not localized in discrete particles but is instead continuously distributed throughout the gravitational field.

The persistent invisibility and intangibility of this form of mass–energy presents a conceptual challenge. However, this difficulty is not entirely new. As noted by Leon Brillouin [37, 36]:

> "There is no energy without mass, but it seems that most authors simply ignored the case of potential energy. The founders of Relativity keep silent about it. As a matter of fact, the corresponding energy is spread all around in space, and so is the mass. Symmetry properties of this distribution suggests splitting the mass fifty-fifty between interacting particles. It is necessary to reevaluate the values of masses, even in the classical theory of relativity, where this consideration was simply ignored. Renormalization is absolutely essential, before quantum theory, and must start at the beginning of Einstein's relativity"

Brillouin's insight underscores a key theoretical omission in classical relativity, the mass-equivalence of potential energy is spatially distributed and cannot be attributed to any single point. This aligns with our interpretation, the gravitational potential energy of a system manifests as an extended, nonlocal mass–energy field. As such, the field itself contributes to the curvature of spacetime, producing the dynamical effects attributed to dark mass.

Field Proportionality and the Localization of Dark Mass

Although the problem of the mass associated with gravitational potential energy was clearly articulated by Brillouin as early as 1952, it has not received a satisfactory treatment in either classical or relativistic physics. In this work, we postulate that the mass stored in the gravitational field is directly proportional to the intensity of the field at a given point.

Let $\Phi(E_a)$ denote the gravitational field contribution from a dark mass E_a at position a, and $\Phi(M_a)$ the field produced by a baryonic mass M_a at the same point. Likewise, at position b, $\Phi(M_b)$ denotes the baryonic field component and $\Phi(E_b)$ the dark field component. We assume the following proportionality relationship:

$$\frac{\Phi(E_b)}{\Phi(E_a)} = \frac{\Phi(M_b)}{\Phi(M_a)}$$

Using the standard expression for the gravitational field produced by a point mass,

$$\Phi(M) \propto \frac{M}{R}$$

where R is the characteristic radius or distance from the source, we obtain:

$$\frac{\Phi(M_b)}{\Phi(M_a)} = \frac{M_b R_a}{M_a R_b} \quad \text{and} \quad \frac{\Phi(E_b)}{\Phi(E_a)} = \frac{E_b R_a}{E_a R_b}$$

Equating the two ratios leads to:

$$\frac{E_b R_a}{E_a R_b} = \frac{M_b R_a}{M_a R_b}$$

which simplifies to:

$$\frac{E_b}{E_a} = \frac{M_b}{M_a} \quad \Rightarrow \quad E_b = E_a \cdot \frac{M_b}{M_a}$$

This relation provides a simple but powerful rule: the local dark mass is proportional to the local baryonic mass, under the assumption that gravitational field strength governs the distribution of field-stored mass–energy.

Component Contributions to Dark Mass Production

In the galactic context, the production of gravitationally induced dark mass must be analyzed component by component, as each baryonic contributor exhibits a different efficiency in generating potential energy. In practice, the available observational data typically separate the baryonic mass into at least two components, the gas mass and the stellar disk mass.

If the gas component contributes to a dark mass E_{gas} from a baryonic mass M_{gas} located at point a, and the stellar disk contributes to E_{disk} from a baryonic mass M_{disk} also located at point a, we compute their relative contributions to the total gravitationally induced dark mass at point b, where local baryonic masses m_{gas} and m_{disk} are present. These can be expressed as:

$$e_{\text{gas}} = \frac{E_{\text{gas}}\, m_{\text{gas}}}{M_{\text{gas}}}, \quad e_{\text{disk}} = \frac{E_{\text{disk}}\, m_{\text{disk}}}{M_{\text{disk}}}$$

The total contribution at point b is then $e_{\text{tot}} = e_{\text{gas}} + e_{\text{disk}}$.

However, this division is still simplistic. As shown earlier, the gravitational potential energy varies significantly depending on stellar type (e.g., red dwarfs, red giants, white dwarfs, black holes). A more accurate treatment would require dividing the baryonic mass into multiple categories, each with distinct mass and density. These variations determine the gravitational binding energy and thus the amount of dark mass effectively "generated" by each category. A coarse two-component model can serve as an approximation, but more detailed modeling is essential for precision.

Two-Component Model with a Single Fitting Parameter

In the absence of detailed information about stellar sub-populations, we limit our analysis to the two dominant baryonic components typically available in observational data, the gas and the stellar disk. Their respective contributions to the gravitationally induced dark mass are modeled using a single free parameter f, which represents the fraction of E_{dark} attributed to the gas component.

The total modeled dark mass is expressed as:

$$E_{\text{dark}} = E_{\text{gas}} + E_{\text{disk}} = fE_{\text{dark}} + (1-f)E_{\text{dark}}$$

From this, we define the relative contributions for each data point as:

$$e_{\text{gas}} = \frac{fE_{\text{dark}}\, m_{\text{gas}}}{M_{\text{gas}}}, \quad e_{\text{disk}} = \frac{(1-f)E_{\text{dark}}\, m_{\text{disk}}}{M_{\text{disk}}}$$

where:

- $E_{\text{dark}}, M_{\text{gas}}, M_{\text{disk}}$ are values measured at the midpoint radius of the galaxy.
- $e_{\text{dark}}, m_{\text{gas}}, m_{\text{disk}}$ are values measured at the data point.

The parameter f is optimized once per galaxy and applied uniformly across all data points. Despite its simplicity, this model reproduces the observed dark mass within the margin of error for 76 of the 175 galaxies in the SPARC sample—corresponding to 43% of the dataset.

To remain conservative in our analysis of the error, we assign to each calculated value e_{tot} the same uncertainty as that of the corresponding observed dark mass e_{dark}. Figures 6a and 6b illustrate representative examples of galaxies well fitted by this single-parameter, two-component model.

Figure 6: Examples of galaxies well fitted by single-parameter, two-component model.

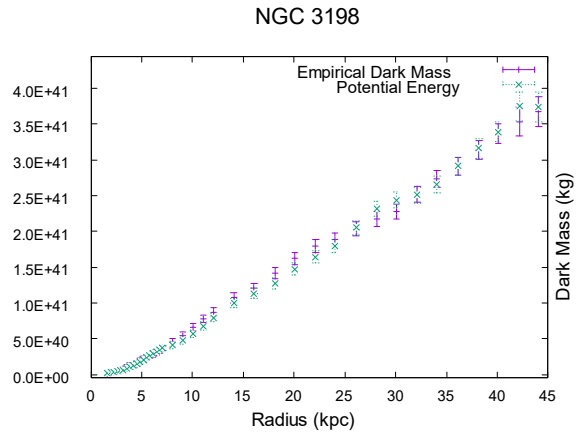

(a) Fitted stellar and gas contributions for NGC 3198.

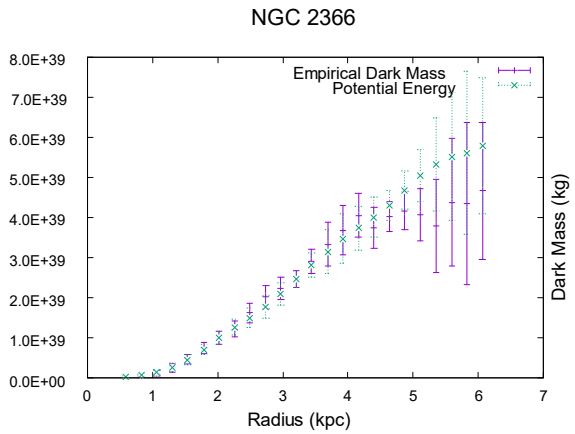

(b) Fitted stellar and gas contributions for NGC 2366.

Incremental Refinement of the Two-Component Model

It is possible to increase the accuracy of the model by introducing additional f parameters, each associated with a distinct radial region of the galaxy. These parameters allow the relative weighting between gas and stellar disk contributions to vary spatially, thereby improving the fit to the observed dark mass profile.

For each segment, the scaling is performed using the midpoint of the segment as the local reference, with its own values of $E_{\text{dark}}, M_{\text{gas}}, M_{\text{disk}}$. This ensures that the calculation within each region remains physically consistent and properly normalized.

Using two f parameters, we achieve error-free fits for 29 additional galaxies. Allowing three f parameters yields an additional 6 galaxies with perfect fits. In total, this approach

provides error-free solutions for 111 out of 175 galaxies, or approximately 63% of the SPARC sample.

The ability to reproduce the observed dark mass distributions across such a large fraction of galaxies—using only local baryonic mass and the ratio of dark mass at different points, interpreted as potential energy stored in the gravitational field—strongly supports the existence of a direct, physically meaningful relationship between baryonic mass and the inferred dark mass. This reinforces the core hypothesis that gravitational potential energy, when correctly modeled, accounts for the so-called dark matter without requiring matter.

Cosmological Implications

In previous models for calculating the gravitational potential energy of self-gravitating systems (galaxies, clusters, etc.), the large-scale direct interaction term between distant bodies was considered negligible (see the section "the potential energy of celestial systems"). This term, of the form $-GmM/d$, where d can be interpreted as the mean separation between bodies, is indeed extremely small on stellar scales. However, at cosmological scales, and when summed over all bodies in the universe, its contribution becomes significant.

Let us consider a set of n point masses of mass m, separated on average by a distance d, for a total mass $M = nm$. The sum of interactions between each mass and the cumulative preceding ones yields a potential energy:

$$\Delta E_{\text{dil}} = \sum_{i=1}^{n-1} \frac{-GmM_i}{d} = -\frac{Gm^2}{d} \sum_{i=1}^{n-1} i = -\frac{Gm^2}{d} \cdot \frac{n(n-1)}{2} \approx -\frac{GM^2}{2d} \quad (\text{for } n \gg 1)$$

This energy describes the "diluted" state of the universe, a configuration of weakly bound masses at large distances. By integrating this term into our potential energy equation we obtain:

$$\Delta E_p = \frac{3G}{5}\left(\frac{M_n^2}{R_n} - \frac{5M_n^2}{6d} - n\frac{m^2}{r}\right) \approx GM_n^2\left(\frac{3}{5R_n} - \frac{1}{2d}\right)$$

Emergent Pressure

A crucial observation is that R is fixed (set by the compactness and chosen density), while d increases with cosmic expansion. Therefore, the gravitational potential energy ΔE_p increases with d (and thus with volume V):

$$\frac{d\Delta E_p}{dV} > 0 \quad \Rightarrow \quad P = -\frac{d\Delta E_p}{dV} < 0$$

This result is interpreted as a negative gravitational pressure, not originating from an exotic scalar field, but from the geometric evolution of a structured gravitational field. As space expands, background gravitational interactions weaken, leading to a growing potential energy. Its negative derivative, with respect to volume, manifests as an effective repulsive

pressure—a natural source of accelerated expansion. This pressure can be expressed as a function of cosmic volume V, assuming R remains constant (galactic structure is assumed stable), and that $d = (3V/4\pi)^{1/3}$:

$$\Delta E_p(V) = GM^2 \left(\frac{3}{5R} - \frac{1}{2(3/4\pi)^{1/3} V^{1/3}} \right)$$

The corresponding effective pressure is:

$$P(V) = -\frac{d\Delta E_p}{dV} = -GM^2 \cdot \frac{1}{2(3/4\pi)^{1/3}} \cdot \frac{1}{3} V^{-4/3} = -\frac{GM^2}{6(3/4\pi)^{1/3} V^{4/3}}$$

To assess the cosmological implications of this effective pressure, we insert it into the Friedmann equations. Assuming a spatially flat universe ($k = 0$):

$$\frac{\ddot{a}}{a} = -\frac{4\pi G}{3} \left(\rho(V) + \frac{3P(V)}{c^2} + 2\,\rho_{\rm rad}(V) \right) + \frac{\Lambda c^2}{3}$$

with:

$$\rho_{\rm rad}(V) = \frac{M_{\rm rad}}{V_0} \left(\frac{V}{V_0} \right)^{-4/3} = M_{\rm rad}\, \frac{V_0^{1/3}}{V^{4/3}}, \qquad P_{\rm rad}(V) = \tfrac{1}{3}\, \rho_{\rm rad}(V)\, c^2$$

Which allows to obtain:

$$\frac{\ddot{V}}{V} = -\frac{A}{V} + \frac{B - C}{V^{4/3}} + \frac{2}{3}\left(\frac{\dot{V}}{V}\right)^2 + \Lambda c^2 \qquad V(a) = V_0\, a^3$$

with:

$$A = 4\pi G\, M_{\rm dust}, \qquad B = \frac{4\pi G^2}{Kc^2}\, M_{\rm gal}^2, \qquad C = 8\pi G\, M_{\rm rad}\, V_0^{1/3}, \qquad K = \left(\frac{3}{4\pi}\right)^{1/3}$$

Negligible Emergent Pressure

(i) B vs. A:

$$\frac{B/V^{4/3}}{A/V} = \frac{G\, M_{\rm gal}^2}{Kc^2\, M_{\rm dust}}\, \frac{1}{V_0^{1/3}}\, \frac{1}{a}$$

At the present epoch ($a = 1$) and with $M_{\rm gal} = 8.70 \times 10^{52}\,\mathrm{kg}$, $M_{\rm dust} = 9.60 \times 10^{53}\,\mathrm{kg}$, $V_0^{1/3} = (4\pi/3)^{1/3} R_{\rm ref}$, $R_{\rm ref} \simeq 5.149 \times 10^{26}\,\mathrm{m}$, we obtain:

$$\left[\frac{B/V^{4/3}}{A/V}\right]_{a=1} \simeq 1.1 \times 10^{-2}$$

Since the ratio $\propto a^{-1}$, one would need to go down to $a_\star \sim 1.1 \times 10^{-2}$ ($z \sim 90$) for B to rival A. Over the whole range of interest ($z \lesssim 10$), B remains $\lesssim 1\%$ of A (and $\ll \Lambda c^2$), hence numerically negligible.

(ii) B vs. C:

$$\frac{C/V^{4/3}}{B/V^{4/3}} \;=\; \frac{C}{B} = \frac{2Kc^2}{G}\,\frac{M_{\rm rad}\,V_0^{1/3}}{M_{\rm gal}^2}$$

The two terms $B/V^{4/3}$ and $C/V^{4/3}$ share the same a^{-4} scaling, so their ratio is constant.

In a standard universe (standard radiation), $\Omega_{r0} \simeq 9\times10^{-5}$ and $\rho_{c0} \simeq 8.66\times10^{-27}\,\mathrm{kg\,m^{-3}}$ give $M_{\rm rad} = \Omega_{r0}\rho_{c0}V_0 \simeq 4.5\times10^{50}\,\mathrm{kg}$. With $V_0^{1/3} \simeq 5.149\times10^{26}\,\mathrm{m}$ and $M_{\rm gal} = 8.70\times10^{52}\,\mathrm{kg}$, we find:

$$\frac{C}{B} \;\simeq\; 5\times10^{-2} \;\ll\; 1$$

i.e. the gravitational potential contribution drowns C today; $C < B \ll A,\ \Lambda c^2$. The threshold for C to overwhelm B is obtained by imposing $C \gtrsim B$, which requires:

$$M_{\rm rad} \;\gtrsim\; \frac{G}{2Kc^2}\,\frac{M_{\rm gal}^2}{V_0^{1/3}} \;\simeq\; 9\times10^{51}\ \mathrm{kg}$$

i.e. $\gtrsim 20$ times the standard radiation. In other words, in a standard universe, C never dominates B. There is no epoch where C and B are simultaneously large enough to be disentangled by background observables.

Cosmological Hypercoincidence

Although the pressure associated with potential energy is negligible, another phenomenon—the decay of dark mass as a function of redshift z—remains critical. Indeed, the production of galactic dark mass decreases systematically with increasing z, simply because there are fewer dense stellar remnants in the past. The potential energy generated therefore reaches only a decreasing fraction of the expected value (Table 7).

We thus immediately see the nature of the *cosmological hypercoincidence*: although potential energy reproduces, with statistical significance greater than 5σ, the dark mass at $z = 0$, it systematically fails at high z.

Table 7: Fraction of the expected ΛCDM galactic dark mass (4.075×10^{53} kg) as a function of redshift z.

z	0	1	2	3	4	5	6	7	8	9	10
DM	100%	96%	88%	77%	62%	41%	27%	21%	15%	12%	11%

One might hope that the phenomenon could be compensated by extragalactic dark mass. In reality, the situation is even more constraining, because the mass of a turnaround block is fixed in general relativity by the Kottler (or Schwarzschild–de Sitter) metric, which imposes a maximal turnaround radius given by

$$R_{\rm ta,max} = \left(\frac{3GM}{\Lambda c^2}\right)^{1/3}$$

At high redshift, however, the expansion is no longer dominated by Λ but by the matter density increasing as $(1+z)^3$. This reduces the effective turnaround radius and, consequently, the mass contained in each cell. Thus, one naturally goes from a typical value of 6×10^{43} kg at $z = 0$ to about 3×10^{43} kg at $z = 1$. This leads to a drastic decrease of the possible extragalactic potential energy (Table 8).

Table 8: Fraction of the expected ΛCDM extragalactic dark mass (4.01×10^{53} kg) as a function of redshift z.

z	0	1	2	3	4	5	6	7	8	9	10
DM	100%	53%	34%	19%	12%	10%	5%	4%	3%	2%	2%

Obviously, such a reduction of mass during cosmological evolution induces a pronounced acceleration that would be perfectly detectable (Figure 7). Moreover, such a decrease of extragalactic dark mass appears strongly incompatible with current models of large-scale structure formation.

The amount of extragalactic dark mass expected on cosmological scales is of the order of 4×10^{53} kg, which corresponds to a fraction of $\sim$ 26–27 % of the universal critical density as inferred from the ΛCDM model. This estimate is consistent with global analyses indicating that dark matter constitutes about 84 % of all matter, compared to only 16 % for baryonic matter [38]. The presence of such a dark mass is essential for understanding large-scale gravitational dynamics and the hierarchical formation of structures [39].

Figure 7: Deceleration parameter $q(z)$ curve with variation of dark mass (potential energy) as a function of z, compared to the ΛCDM model.

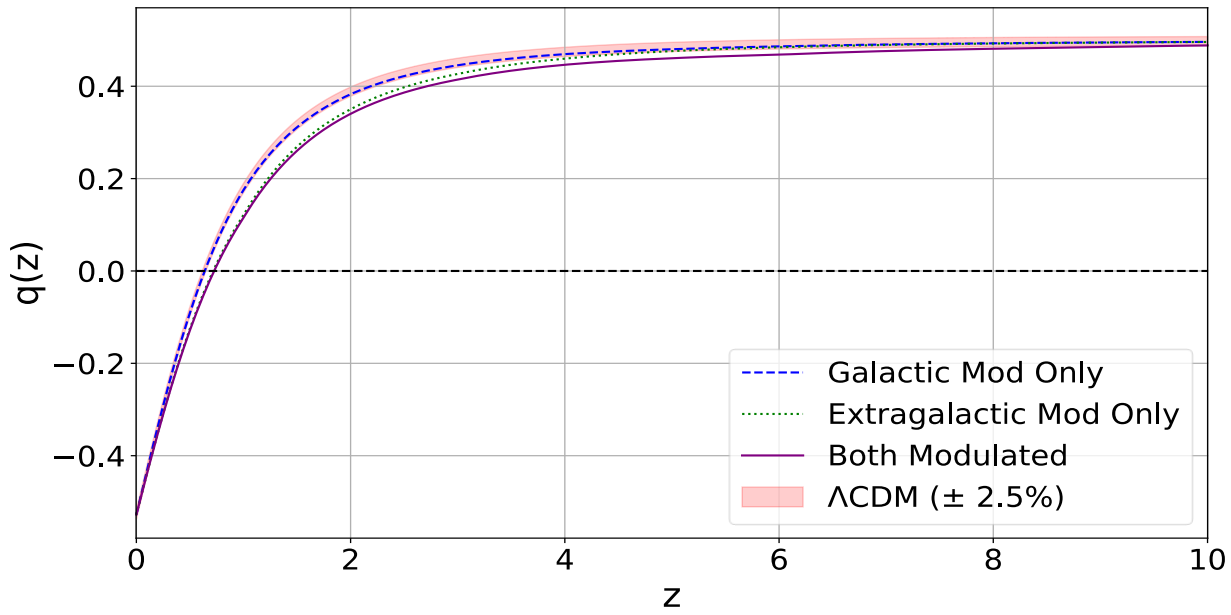

Thermodynamic Reconciliation of General Relativity

Our theoretical framework faces a fundamental difficulty: it accurately describes the present epoch, but does not satisfactorily reproduce past evolution. A second point concerns the first law of thermodynamics. In general relativity, *local* conservation is guaranteed by $\nabla_\mu T^{\mu\nu} = 0$, but *global* energy is not generally defined in the absence of temporal symmetry (no timelike Killing vector field in an expanding universe), as formalized by Noether's theorem. In other words, the lack of global conservation does not contradict GR; it is a geometric consequence of it.

In order to reconcile gravitational dynamics with a global conservation principle, we introduce an axiom of extended conservation of quasi-local energy, in which variations of gravitational potential energy are compensated by vacuum energy through a variable effective cosmological constant. Written in covariant form, this hypothesis corresponds to an evolution of Λ such that:

$$\nabla_\mu T^{\mu\nu} \;=\; -\frac{c^4}{8\pi G}\,\nabla^\nu \Lambda \qquad \Longleftrightarrow \qquad \nabla_\mu \Big(T^{\mu\nu} + T^{\mu\nu}_{(\Lambda)} \Big) = 0$$

with $T^{\mu\nu}_{(\Lambda)} = -\,\frac{\Lambda c^4}{8\pi G}\, g^{\mu\nu}$. In a comoving volume, one then imposes a global conservation law:

$$\frac{d}{dt}\Big(E_{\rm pot} + E_\Lambda \Big) = 0, \qquad E_\Lambda \equiv \rho_\Lambda c^2 V, \quad \rho_\Lambda = \frac{\Lambda c^2}{8\pi G}$$

which allows regulated exchanges between gravitational potential energy and vacuum energy. Such a scheme aims to address simultaneously (i) the apparent thermodynamic tension and (ii) the cosmological "coincidence," while preserving the covariant consistency of the formalism.

Extended conservation and exchange with the vacuum — We postulate that the dynamics include an effective vacuum energy $\rho_\Lambda(t) = \Lambda(t)c^2/(8\pi G)$ which exchanges energy with dark mass (DM). At the covariant level:

$$\nabla_\mu \big(T^{\mu\nu}_{\rm dm} + T^{\mu\nu}_{\rm b} + T^{\mu\nu}_{(\Lambda)} \big) = 0, \qquad T^{\mu\nu}_{(\Lambda)} = -\,\frac{\Lambda c^4}{8\pi G}\, g^{\mu\nu}$$

In a homogeneous and isotropic FLRW spacetime, this yields the coupled continuity equations:

$$\dot\rho_{\rm dm} + 3H\rho_{\rm dm} = +Q, \qquad \dot\rho_\Lambda = -Q$$

where Q encodes the energy exchange (positive if the vacuum provides energy to DM). If one imposes a constant ratio:

$$r \;\equiv\; \frac{\rho_\Lambda}{\rho_{\rm dm}} = \kappa = \text{constant} > 0$$

then $\rho_\Lambda = \kappa\,\rho_{\rm dm}$ and the system becomes:

$$(1+\kappa)\,\dot\rho_{\rm dm} + 3H\rho_{\rm dm} = 0 \;\;\Longrightarrow\;\; \rho_{\rm dm}(a) = \rho_{\rm dm,0}\, a^{-3/(1+\kappa)} \quad \rho_\Lambda(a) = \kappa\,\rho_{\rm dm}(a)$$

The corresponding coupling is $Q = -\dot\rho_\Lambda = \kappa\,\dot\rho_{\rm dm} = -\frac{3\kappa}{1+\kappa} H\rho_{\rm dm}$. Thus, the vacuum energy remains of the same order of magnitude as DM at all redshifts ("hypercoincidence" constraint).

Turnaround condition and block mass — In the vicinity of a bound system, the Kottler metric (Schwarzschild–de Sitter) gives the radial equilibrium (non-relativistic test):

$$\ddot{R} \;=\; -\frac{GM}{R^2} + \frac{\Lambda_{\text{eff}} c^2}{3}\, R$$

The turnaround radius R_{ta} satisfies $\ddot{R} = 0$, hence:

$$R_{\text{ta}}^3 \;=\; \frac{3GM}{\Lambda_{\text{eff}} c^2}$$

We define the turnaround mass of the block as $M_{\text{ta}} \equiv M(R_{\text{ta}})$. In the standard scenario (Λ constant, hierarchical growth), $M_{\text{ta}}(z)$ varies strongly with z. Here, we impose the constraint:

$$\frac{M_{\text{ta}}(z)}{\Lambda_{\text{eff}}(z)} \;=\; \frac{M_{\text{ta}}(0)}{\Lambda_{\text{eff}}(0)} \;=\; \text{constant}$$

so that, for a reference R_{ta} (or a normalization at $z = 0$):

$$M_{\text{ta}}(z) \;=\; M_{\text{ta}}(0) \quad \text{(constant)}$$

In other words, the variation of $\Lambda_{\text{eff}}(z)$ compensates the evolution that, in ΛCDM, would make M_{ta} vary. We fix the normalization by $M_{\text{ta}}(0) = 6.0 \times 10^{43}$ kg and choose $\Lambda_{\text{eff}}(z)$ so as to keep $M_{\text{ta}}(z) = M_{\text{ta}}(0)$.

Global (quasi-local) coherence — In a comoving volume V, we postulate an extended global conservation law:

$$\frac{d}{dt}\Big(E_{\text{pot}} + E_\Lambda\Big) = 0, \qquad E_\Lambda \equiv \rho_\Lambda c^2 V$$

where E_{pot} is the quasi-local gravitational potential energy (e.g. the Brown–York term at fixed surface). Writing $dE_{\text{pot}} = -\,dE_\Lambda$, one recovers at the level of densities the relation $\dot{\rho}_\Lambda = -Q$ introduced above, which makes the compensation through $\Lambda_{\text{eff}}(z)$ consistent and ensures (i) a constant ratio $\rho_\Lambda/\rho_{\text{dm}}$ (hypercoincidence), and (ii) a constant turnaround mass $M_{\text{ta}}(z) \equiv M_{\text{ta}}(0)$, thus a fixed value (here 6.0×10^{43} kg) at all redshifts.

Reconciliation with Cosmological History

Since the turnaround mass remains fixed at its $z = 0$ value of 6.00×10^{43} kg, a remarkable phenomenon appears, the extragalactic dark mass also remains constant. Thus, even if our fusion algorithm highlights, at different z, significant energetic discrepancies at the level of individual galaxies, these discrepancies cancel out once we consider the fusion of groups of galaxies. Indeed, although variations in stellar density locally generate notable differences, the complete fusion of the stars within a galaxy leads to compact balls whose densities remain fairly similar at any z, since the fraction of very dense stars is relatively small. It

is therefore natural that the fusion of balls with comparable densities produces similar dark masses. Consequently, the same turnaround cells are recovered at all redshifts (Table 6).

However, since the extragalactic dark mass ($M_{\rm edark}$) remains constant while the galactic dark mass ($M_{\rm gdark}$) decreases with increasing redshift, their ratio $M_{\rm gdark}/M_{\rm edark}$ also decreases with z (Table 9).

Table 9: Evolution of the ratio $M_{\rm gdark}/M_{\rm edark}$ as a function of redshift.

z	0	1	2	3	4	5	6	7	8	9	10
$\frac{M_{\rm gdark}}{M_{\rm edark}}$	102%	98%	90%	78%	63%	42%	28%	22%	15%	12%	10%

We might believe that this should lead to an apparent inconsistency with the standard ΛCDM model; however, this is not the case, and this framework provides a natural explanation for several phenomena. A non-exhaustive list follows:

Current tensions arise less from the total amount of dark mass than from its partition between components bound to galactic halos and diffuse extragalactic reservoirs. Many state-of-the-art hydrodynamical simulations (Illustris, EAGLE, TNG) tend to concentrate too large a fraction of both mass and baryons within central galaxies, which results in excessive stellar production and, correspondingly, in an underestimated reservoir of diffuse hot gas at the scale of groups, clusters, and filaments [46, 45, 47, 48, 49]. On the observational side, baryon budgets derived from UV/X absorptions, SZ, and X-ray measurements converge toward a picture in which the extragalactic baryonic mass (CGM/ICM + hot IGM/WHIM) largely dominates at $z = 0$ [40, 41, 42, 44], in agreement with global cosmological constraints [43]. This observation/simulation asymmetry suggests that the *galactic/extragalactic ratio* is systematically *overestimated* in current numerical models.

Reducing the ratio $M_{\rm gdark}/M_{\rm edark}$ simultaneously alleviates several of these tensions. From a dynamical perspective, redistributing dark mass toward the meso-scale environment (groups/filaments) strengthens the gravitational potential at ~ 0.5–3 Mpc while loosening the grip at galactic centers, thereby limiting the capture of cold gas and the overproduction of stars [47, 48]. From the thermodynamic perspective of baryons, a more massive extragalactic reservoir more naturally confines and sustains the hot CGM/ICM/IGM, bringing observed inventories (HST/COS, SZ, X-ray) closer to expected budgets [40, 41, 44]. Finally, from a cosmographic perspective, heavier environments stabilize turnaround physics over cosmic history, preventing too rapid a drop in effective extragalactic mass at high redshift, while allowing the galactic component to decline with z as suggested by the data.

This scheme leads to consistent observable signatures. A more dominant extragalactic environment implies a stronger two-halo term and enhanced gravitational shear at meso-scales, stronger SZ/kSZ signals in bridges between halos and along filaments, and larger CGM/ICM masses consistent with absorption and scattering measurements [44, 40, 41]. It preserves the overall ΛCDM framework (CMB/BAO/large-scale structure), while readjusting the partition of dark mass at the scales where tensions appear. In this sense, a smaller $M_{\rm gdark}/M_{\rm edark}$ ratio provides a unified explanation for local and meso-scale divergences without compromising the fundamental cosmological successes.

Conclusion

The objective of this article was to demonstrate that the phenomenon commonly referred to as "dark matter" can be fully accounted for by gravitational potential energy. Through both theoretical and empirical approaches, we have shown that the potential energy generated by gravitational interactions—particularly when applied to systems like the Earth–Moon or Earth–Sun—is far from negligible and must be considered as a real, physical quantity.

Using simplified theoretical models, we established that this potential energy, when converted via the mass–energy equivalence relation $E = mc^2$, yields contributions on the same order of magnitude as the dark mass inferred from galactic rotation curves.

We subsequently compared our theoretical model to a substantial body of observational data and obtained an excellent fit, despite the necessarily simplified assumptions used throughout. This empirical success provides a necessary condition for validating the model: the gravitational potential energy predicted by the distribution of baryonic mass must be sufficient to account for the observed dark mass. Our results show that this condition is fulfilled across a wide range of galaxy types.

We then extended our model by applying the principle of causal proportionality—namely, that identical mass distributions of the same type must generate proportionally identical effects. If a baryonic mass M, composed of stars of a given type (e.g., solar-mass stars), produces a corresponding dark mass E, then a subcomponent of mass m will generate a dark mass:

$$e = \frac{Em}{M}$$

When expressed as a gravitational field, this implies that the spatial distribution of dark mass follows the distribution of baryonic mass—provided that the composition (stellar types, gas fraction) remains homogeneous. This directly recovers the empirically observed correlation between baryonic and dark mass profiles [50, 51], but here it arises naturally as a consequence of the gravitational field's structure, rather than requiring a phenomenological assumption.

Thus, the hypothesis that dark mass is generated by gravitational potential energy not only accounts for its magnitude but also provides a fundamental explanation for its spatial distribution. What had previously appeared mysterious—the alignment between baryonic and dark matter—is shown here to be the logical consequence of field–based mass–energy equivalence.

Finally, it is straightforward to apply the same method as for SPARC, but on the cosmological scale, in order to compute the total galactic dark mass of the Universe. Moreover, this same gravitational potential energy makes it possible to establish a functional relation between the turnaround radius and the extragalactic dark mass, and to calculate it precisely.

The probability that these combined elements can explain the dark universe has been conservatively estimated at a significance level greater than 5σ. It should be emphasized that this estimate does not even consider the conceptual simplicity of the proposed model, nor the fact that gravitational potential energy is a well-established physical quantity, commonly used in engineering and classical physics.

Our success in explaining dark mass through gravitational potential energy with such high precision at the present epoch unfortunately fails in the cosmological past. This failure, however, does not undermine the 5σ statistical significance of our results; rather, it calls for an additional explanation.

A simple and natural solution is to adjust the cosmological constant so as to exactly compensate for the decrease of dark mass in the past. This idea, far from being new, has already been considered within frameworks such as quintessence or cosmological backreaction. However, none of these approaches has yet provided a direct and robust adaptation to observational constraints.

By postulating the equivalence between dark mass and the total gravitational potential energy of the Universe, this adjustment is not ad hoc: on the contrary, it represents a way to reconcile general relativity with the first law of thermodynamics, since the total energy of a closed system such as the Universe must remain conserved.

Thus, what initially appeared as a failure is in fact the manifestation of a deeper conservation principle, unifying general relativity with the rest of physics under the same thermodynamic constraints. At the same time, it naturally explains the cosmological coincidence problem.

The Problem of the Epistemological Obstacle

Perhaps the most profound question raised by this work is why the role of gravitational potential energy in generating dark mass has remained unrecognized for so long. Both gravitational potential energy and the mass–energy equivalence relation $E = mc^2$ are well-established principles, each supported by extensive experimental validation. Moreover, the concept of binding energy contributing to mass is not new. Nuclear binding energy, for example, is well understood as a measurable mass defect in atomic systems, though its localization is typically attributed to the quantum field.

The primary reason gravitational binding energy has been historically dismissed as a source of mass is the perception that gravity is too weak a force to produce significant energy effects. However, our results challenge this assumption. While nuclear binding energy yields modest contributions to mass on the scale of atomic nuclei—often a few percent—gravitational potential energy can generate dark mass equivalents many times greater. In galactic systems, the ratio of gravitational potential energy to baryonic mass can exceed a factor of ten, and in clusters or larger structures, this ratio can be much higher.

This contrast highlights a scale-dependent truth: gravity is weak on the quantum scale but becomes dominant on astronomical scales, while the strong nuclear force behaves inversely. Immense at the subatomic level but negligible beyond the nucleus. The failure to account for this scale dependence may explain why the gravitational origin of dark mass has remained obscured, despite the knowledge of the theoretical and empirical tools needed to uncover it.

Another major conceptual obstacle to recognizing the gravitational origin of dark mass lies in the widespread use of Newton's second theorem. Indeed, it allows a solid sphere to be

considered as a point mass. This simplification naturally comes to mind when studying large stellar systems and has led to a poor understanding of what useful gravitational potential energy is. Traditional approaches focus on the relative position of celestial bodies, considered as point masses, emphasizing the term $E = -GmM/d$ as the main contribution. However, as we have demonstrated, this term is negligible compared to the energy associated with a restructuring of the system—here, the merger or separation of massive bodies—under conservation of volume density.

The useful potential energy does not result solely from distance, but from the energy difference between two distinct macroscopic states of the system. It is this transformation of state, respecting the physical properties of matter, that reveals the true energy content of the gravitational field. The historical focus on positional interaction, rather than on the internal reorganization of masses, has contributed to masking the role of potential energy as the real source of space–time curvature. By reconsidering potential energy as a quantity localized in the field and generating mass, we find a physically coherent explanation of the dark mass phenomenon—already contained in classical gravitational theory, but which has remained unnoticed due to a discreet but decisive conceptual bias.

Challenge of General Relativity and Theoretical Implications

A deeper theoretical difficulty lies in the fact that Newtonian gravity (GN) is not the fundamental theory of gravitation—General Relativity (GR) is. Unlike GN, GR does not admit a general, global conservation law for energy. As Emmy Noether showed, conservation of energy in GR only holds under very specific symmetries, such as time-translation invariance, which do not apply in dynamically evolving spacetimes. In particular, the notion of gravitational potential energy, central to Newtonian dynamics, does not have a direct, covariant analog in GR.

This creates a conceptual tension, if a phenomenon as significant as the dark mass arises from gravitational potential energy, and this energy is absent or ill-defined in GR, then one must ask why Newtonian theory—a weak–field approximation—appears to succeed where the full relativistic theory offers no equivalent formulation. The challenge is philosophical as well as physical.

Nevertheless, GN remains extraordinarily accurate in the weak–field regime and is vastly simpler to work with than GR. The dynamics of galaxies, where the gravitational field is weak and velocities are non-relativistic, fall squarely into this domain. In Newtonian gravity, the potential energy of the system is known, but to determine the correct dynamics, that energy must be reintroduced into the system—that is, it must be treated as a source of gravity. It is difficult to believe that GR would yield significantly better results unless the issue lies in an incomplete accounting of gravitational self-induction—the field's interaction with its own energy density [52, 53, 55, 54]. If this is indeed the case, then the most natural resolution would be to find a weak–field expansion of GR in which this self-induction appears explicitly. In such a formulation, the gravitational potential energy term should re-emerge, but now as a derived, not postulated, quantity.

More speculatively, the fact that gravity "recognizes" all forms of energy—including gravitational potential energy, long regarded as a mere computational artifact—suggests the existence of a deeper unifying principle. The Higgs field already hints at such a principle in a limited domain, it translates scalar potential energy into inertial mass for certain particles. Gravity appears to generalize this mechanism, coupling not just to scalar fields but to all forms of energy—kinetic, electromagnetic, nuclear, or gravitational.

The fundamental problem of the coupling of gravitational energy to other fields remains that energy is not conserved in GR. A striking example is the fact that the potential energy decreases with redshift in our model. However, the non-existence of an invariance does not mean the non-existence of a phenomenon, on the contrary, it is even more interesting because of its variation. The problem amounts to introducing a variation into a physics based on invariance. Moreover, potential energy is a global phenomenon that is difficult to reconcile with a local phenomenon. Fortunately, renormalization remains as a mechanism for scale adjustment.

Final Remarks

In conclusion, the study of dark mass does not seem to require an alternative theory of gravitation or exotic particles. Here, even general relativity might prove unnecessary in this context, the framework of classical Newtonian mechanics, extended to the mass–energy equivalence $E = mc^2$, seems sufficient.

We have demonstrated that simple, physically grounded models can accurately reproduce the magnitude and distribution of dark mass in a wide range of galactic systems. These models can be systematically improved—for example, by incorporating a detailed synthesis of stellar populations, a more accurate treatment of interstellar gas, or a more refined modeling of radial distributions. The same methodology may also be extended to larger cosmic structures such as galaxy clusters and superclusters.

Furthermore, the mixed use of general relativity and classical calculation of potential energy seems necessary for a correct understanding of the phenomenon attributed to dark energy. Here too, an improvement of the model seems necessary.

One conclusion is unavoidable: gravitational potential energy can no longer be neglected in discussions on dark mass and dark energy. Its inclusion provides both a quantitative and conceptual solution to a long-standing astrophysical mystery.

The C++ and Python programs used to perform all numerical calculations and generate the corresponding graphs are freely available at `dark-mass-generator.sourceforge.io`.

Funding Statement

This research received no specific grant from any funding agency in the public, commercial, or not-for-profit sectors.

References

[1] Rubin, V. C. and Ford, W. K., Jr. (1970). *Rotation of the Andromeda Nebula from a Spectroscopic Survey of Emission Regions*. Astrophysical Journal, **159**, 379 – 404.

[2] Rubin, V. C., Ford, W. K., Jr. and Thonnard, N. (1980). *Rotational Properties of 21 Sc Galaxies with a Large Range of Luminosities and Radii from NGC 4605 (R = 4 kpc) to UGC 2885 (R = 122 kpc)*. Astrophysical Journal, **238**, 471 – 487.

[3] Rubin, V. C., Burstein, D., Ford, W. K., Jr. and Thonnard, N. (1985). *Rotation Velocities of 16 Sa Galaxies and a Comparison of Sa, Sb, and Sc Rotation Properties*. Astrophysical Journal, **289**, 81 – 104.

[4] Gondolo, P., et al. (1997). *AGAPE: a Microlensing Search for Dark Matter by Monitoring Pixels*, in Dark and Visible Matter in Galaxies, ASP Conference Series, Vol. 117.

[5] Alcock, C., et al. (2000). *The MACHO Project: Microlensing Results from 5.7 Years of LMC Observations*. Astrophysical Journal, **542**, 281 – 307.

[6] Tisserand, P., et al. (2007). *Limits on the Macho Content of the Galactic Halo from the EROS-2 Survey of the Magellanic Clouds*. Astronomy & Astrophysics, **469**, 387 – 404.

[7] LUX Collaboration (2017). *Results from a search for dark matter in the complete LUX exposure*. Physical Review Letters, **118**, 021303.

[8] PICASSO Collaboration (2017). *Final results of the PICASSO dark matter search experiment*. Astroparticle Physics, **90**, 85 – 92.

[9] PICO Collaboration (2019). *Dark matter search results from the complete exposure of the PICO-60 C_3F_8 bubble chamber*. Physical Review D, **100**, 021101.

[10] SuperCDMS Collaboration (2023). *Search for low-mass dark matter via bremsstrahlung radiation and the Migdal effect in SuperCDMS*. Physical Review D.

[11] Zhang, P., et al. (2007). *Probing Gravity at Cosmological Scales by Measurements which Test the Relationship between Gravitational Lensing and Matter Overdensity*. Physical Review Letters, **99**, 141302.

[12] Reyes, R., et al. (2010). *Confirmation of general relativity on large scales from weak lensing and galaxy velocities*. Nature, **464**, 256 – 258.

[13] Vegetti, S., et al. (2024). *Strong Gravitational Lensing as a Probe of Dark Matter*. Space Science Reviews, **220**.

[14] MICROSCOPE Collaboration (2022). *Microscope Mission: Final Results of the Test of the Equivalence Principle*. Physical Review Letters, **119**, 121101.

[15] Buonanno, A. and Damour, T. (2000). *Transition from inspiral to plunge in binary black hole coalescences*. Physical Review D, **62**, 064015.

[16] Berti, E., Cardoso, V. and Will, C. M. (2006). *Gravitational-wave spectroscopy of massive black holes with the space interferometer LISA*. Physical Review D, **73**, 103520.

[17] Rezzolla, L., et al. (2008). *Final spin from the coalescence of two black holes*. Physical Review D, **78**, 044002.

[18] Tichy, W. and Marronetti, P. (2008). *Final mass and spin of black-hole mergers*. Physical Review D, **78**, 084038.

[19] Sicilia, A., et al. (2022). *The Black Hole Mass Function Across Cosmic Times. I. Stellar Black Holes and Light Seed Distribution*. Astrophysical Journal, **924**, L2.

[20] Lelli, F., McGaugh, S. S. and Schombert, J. M. (2016). *SPARC: Mass Models for 175 Disk Galaxies with Spitzer Photometry and Accurate Rotation Curves*. Astronomical Journal, **152**, 157.

[21] Bochanski, J. J., Hawley, S. L., Covey, K. R., West, A. A., Reid, I. N., Golimowski, D. A. and Ivezić, Ž. (2010). *The Luminosity and Mass Functions of Low-Mass Stars in the Galactic Disk. I. The Calibration Sample and Luminosity Function*. Astronomical Journal, **139**, 2679.

[22] Holberg, J. B., Sion, E. M., Oswalt, T., McCook, G. P., Foran, S. and Subasavage, J. P. (2008). *A New Look at the Local White Dwarf Population*. Astronomical Journal, **135**, 1225.

[23] Chabrier, G. (2003). *Galactic Stellar and Substellar Initial Mass Function*. Publications of the Astronomical Society of the Pacific, **115**, 763.

[24] Kroupa, P. (2001). *On the variation of the initial mass function*. Monthly Notices of the Royal Astronomical Society, **322**, 231.

[25] Bruzual, G. and Charlot, S. (2003). *Stellar population synthesis at the resolution of 2003*. Monthly Notices of the Royal Astronomical Society, **344**, 1000.

[26] Conroy, C., Gunn, J. E. and White, M. (2009). *The Propagation of Uncertainties in Stellar Population Synthesis Modeling*. Astrophysical Journal, **699**, 486.

[27] Conroy, C. and Gunn, J. E. (2010). *The Propagation of Uncertainties in Stellar Population Synthesis Modeling. II*. Astrophysical Journal, **712**, 833.

[28] Maraston, C. (2005). *Evolutionary population synthesis: models, analysis of the ingredients and application to high-z galaxies*. Monthly Notices of the Royal Astronomical Society, **362**, 799.

[29] Eldridge, J. J. and Stanway, E. R. (2009). *Spectral population synthesis including massive binaries*. Monthly Notices of the Royal Astronomical Society, **400**, 1019.

[30] Stanway, E. R. and Eldridge, J. J. (2018). *Re-evaluating old stellar populations*. Monthly Notices of the Royal Astronomical Society, **479**, 75.

[31] Madau, P. and Dickinson, M. (2014). *Cosmic Star-Formation History*. Annual Review of Astronomy and Astrophysics, **52**, 415.

[32] Pavlidou, V., & Tomaras, T. N. (2014). *Where the world stands still: turnaround as a strong test of ΛCDM cosmology*. Journal of Cosmology and Astroparticle Physics, **09**, 020.

[33] Tanoglidis, D., Nesseris, S., & Pavlidou, V. (2015). *Testing ΛCDM cosmology at turnaround: where to look for violations of the bound?* Journal of Cosmology and Astroparticle Physics, **12**, 060.

[34] Yang, X., Mo, H. J., van den Bosch, F. C., Pasquali, A., Li, C., & Barden, M. (2007). *Galaxy Groups in the SDSS DR4: I. The Catalogue and Basic Properties*. The Astrophysical Journal, **671**, 153.

[35] Kravtsov, A. V., & Borgani, S. (2012). *Formation of Galaxy Clusters*. Annual Review of Astronomy and Astrophysics, **50**, 353.

[36] Brillouin, L. (1964). *L'Enigme $E = Mc^2$: Énergie potentielle et renormalisation de la masse*. Journal de Physique, **25**, 10.

[37] Brillouin, L. (1952). *The actual mass of potential energy, a correction to classical relativity*. Proceedings of the National Academy of Sciences, **53**, 3.

[38] Particle Data Group (2023). "Dark Matter", *Review of Particle Physics*, `https://pdg.lbl.gov/2023/reviews/rpp2023-rev-dark-matter.pdf`.

[39] National Research Council (2003). *Connecting Quarks with the Cosmos: Eleven Science Questions for the New Century*. Washington, DC: The National Academies Press. `https://nap.nationalacademies.org/read/10079/chapter/7`.

[40] Werk, J. K., et al. (2014), *The COS-Halos Survey: Physical Conditions and Baryonic Mass in the Low-Redshift Circumgalactic Medium*, ApJ, **792**, 8.

[41] Tumlinson, J., Peeples, M. S., & Werk, J. K. (2017), *The Circumgalactic Medium*, ARA&A, **55**, 389.

[42] Shull, J. M., Smith, B. D., & Danforth, C. W. (2012), *The Baryon Census in a Multiphase Intergalactic Medium*, ApJ, **759**, 23.

[43] Planck Collaboration (2016), *Planck 2015 results. XIII. Cosmological parameters*, A&A, **594**, A13.

[44] de Graaff, A., Cai, Y.-C., Heymans, C., & Peacock, J. A. (2017), *Missing baryons in the cosmic web revealed by the Sunyaev–Zel'dovich effect*, Science, **358**, 1558.

[45] Crain, R. A., et al. (2015), *The EAGLE simulations of galaxy formation: calibration of subgrid physics and model variations*, MNRAS, **450**, 1937.

[46] Genel, S., et al. (2014), *The Illustris simulation: the evolving population of galaxies*, MNRAS, **445**, 175.

[47] Springel, V., et al. (2018), *First results from the IllustrisTNG simulations: matter and galaxy clustering*, MNRAS, **475**, 676.

[48] Pillepich, A., et al. (2018), *Simulating galaxy formation with the IllustrisTNG model*, MNRAS, **473**, 4077.

[49] Nelson, D., et al. (2018), *The IllustrisTNG simulations: public data release*, MNRAS, **475**, 624.

[50] McGaugh, S. S., Lelli, F. and Schombert, J. M. (2016). *The Radial Acceleration Relation in Rotationally Supported Galaxies*. Physical Review Letters, **117**, 201101.

[51] Lelli, F., et al. (2017). *One Law to Rule Them All: The Radial Acceleration Relation of Galaxies*. Astrophysical Journal, **836**, 152.

[52] Deur, A. (2019). *An explanation for dark matter and dark energy consistent with the standard model of particle physics and General Relativity*. European Physical Journal C, **79**, 883.

[53] Deur, A., Sargent, C. and Terzic, B. (2020). *Significance of Gravitational Nonlinearities on the Dynamics of Disk Galaxies*. Astrophysical Journal, **896**, 94.

[54] Deur, A. (2022). *Effect of the field self-interaction of General Relativity on the cosmic microwave background anisotropies*. Classical and Quantum Gravity, **39**, 13.

[55] Deur, A. (2021). *Relativistic corrections to the rotation curves of disk galaxies*. European Physical Journal C, **81**, 213.